Tropical Cyclones in Changing Climate

44

Hiroyuki Murakami

Contents

Abstract

Tropical cyclones are a highly destructive type of natural disaster. The effect of anthropogenic climate changes on global tropical cyclone activity is of great interest and an important topic among the science community and public. However, little is known about whether the ongoing climate changes have already affected the observed tropical cyclone activity. Despite the lack of a reliable long-term global observed tropical cyclone record, some recent observational and modeling studies have shown clear trends in tropical cyclone activity that could be attributable to anthropogenic climate changes. This chapter introduces those among these recent studies that have not been covered in previous review articles. These include recent observed trends in tropical cyclone activity, new modeling techniques to identify the cause of extreme tropical cyclone events, and new studies on projected future increases in global tropical cyclone numbers. Specifically, significant trends have been unearthed in the spatial distributions of tropical cyclones at the global scale, as well as in terms of an increased frequency of tropical cyclone occurrence in coastal regions worldwide since the 1980s.

H. Murakami (✉)
Geophysical Fluid Dynamics Laboratory, Princeton, NJ, USA
e-mail: Hiroyuki.Murakami@noaa.gov

H. Akimoto, H. Tanimoto (eds.), *Handbook of Air Quality and Climate Change*,
https://doi.org/10.1007/978-981-15-2760-9_34

Some modeling studies indicate that these observed trends could be attributable to some combination of changes in greenhouse gases, anthropogenic aerosols, and volcanic aerosols. There have also been some new studies that have applied the method of event attribution to estimate the influence of anthropogenic climatic changes on extreme storm events or seasons. Some recent studies have reported projected future increases in global tropical cyclone numbers, which is different from previous studies that showed projected decreases, highlighting the substantial level of uncertainty in future projections. This chapter reviews these new studies and discusses their implications and uncertainties.

Keywords

Tropical cyclone · Anthropogenic climate change · Event attribution · Future projection · Uncertainty

1 Introduction

Global mean temperature has been rising rapidly since the mid-twentieth century, and it is widely accepted that a substantial part of this temperature rise is attributable to increases in emissions of greenhouse gases [1]. Meanwhile, the effect of global warming on global tropical cyclone (TC) activity is of great interest and an important topic among the science community. In the last decade, there were many intense TCs that made landfall over coastal regions all over the world, thus stimulating public interest regarding the impact of the ongoing issue of global warming on TC activity. The latest studies indicate that these recent changes in TC activity could be due to human influences on the climate. However, this view has been challenged for the following reasons: (1) the limited availability of long-term TC observations makes it difficult to infer the effect of anthropogenic climate forcing agents on TC activity and (2) the significant influence of intrinsic internal variability on TC activity makes the signal of anthropogenic climatic changes in TC activity difficult to detect.

To discuss the reasons for long-term changes in observed TC activity, enduring and reliable records of TCs are necessary. In this respect, reliable measurements of TC intensities at the global scale have been available since the beginning of the 1980s via satellite visible and infrared images through the Dvorak technique [2]. However, before the satellite era, TCs were mainly observed by ships, land-based observations, and reconnaissance aircraft. Therefore, prior to the meteorological satellite era, TCs that did not approach land or encounter a ship or aircraft had a greater chance of not being detected, leading to missing storms in the observed record. Even after the start of the satellite era, the satellites that have been available have been changing decade by decade. Also, because the Dvorak technique has been changing decade by decade too, the TC data gathered over the years naturally contain temporal heterogeneities, especially the record of storm intensity [3]. In addition, TCs have been analyzed by different organizations with varying methods applied from basin to basin. Therefore, there is an inherent lack of temporal and

spatial consistency in the observed TC data record. In short, the way in which the observed TC data currently available and their associated analysis techniques have evolved has given rise to substantial uncertainty in any trend revealed by them.

Meanwhile, there is also significant internal variation in TC activity at the decadal time scale, which makes it difficult to detect secular trends due to any anthropogenic climate change from the observations. For example, the observed number of TCs shows substantial multi-decadal oscillations in the western North Pacific (WNP) and North Atlantic (NA), revealing significant changes around 1998. Coincidentally, the Pacific Decadal Oscillation (PDO) [4], Interdecadal Pacific Oscillation (IPO) [5], and Atlantic Multidecadal Variability (AMV) [6], which are the known examples of climate variability at the decadal time scale, experienced a change in sign around 1998. Previous studies have reported that the IPO, PDO, and AMV might influence TC activity on the global scale [7–10]. Therefore, several studies have argued that the observed trends in TC intensity and frequency are mainly due to the intrinsic decadal internal variability, as the interpretation of the above decadal variations as natural variability [e.g., 11, 12]. Overall, currently, there is no firm confidence or consensus within the science community regarding the influence of anthropogenic climate change on the observed trends in TC activity, largely due to the substantial uncertainty in the observed TC record and the possibly substantial influence of internal variability [13].

Despite the limitations involved, many studies have attempted to detect observed climate changes in TC activity (i.e., establish that observed changes are highly unusual compared to expected natural variability) using numerical dynamical climate models as well as various observed and reanalysis datasets. A comprehensive review of studies published up to 2019 is available in Knutson et al. [13] from the perspective of observed climate changes in TC activity and in Knutson et al. [14] regarding the possible changes in TC activity projected in the future. However, there have been new studies published since these works by Knutson et al. that are also relevant towards developing an understanding of the effect of anthropogenic climate change on TC activity. The focus in this chapter, therefore, is to review these new studies and discuss their implications and uncertainties. Hereafter, the term "TCs" refers to all storm types, including tropical storms ($\geq$34 kt), hurricanes and typhoons ($\geq$64 kt), and major hurricanes (MHs) ($\geq$96 kt).

2 Detected Climatic Change in the Global Distribution of TCs

TC seasons with unprecedented characteristics have tended to occur all over the world in the most recent decade. For example, the NA experienced a record 30 TCs in 2020; the WNP experienced its first instance of no TCs in July in 2020 [15]; the Central Pacific, including Hawaii, experienced an unprecedented number of TCs and MHs in 2015 [16]; and the Arabian Sea experienced its first instance of multiple intense storms in the post-monsoon season in 2015 [17]. Figure 1a shows the observed trend in TC frequency of occurrence (TCF) over the period 1980–2018. Here, TCF, which can also be referred to as the TC density, is defined as the total

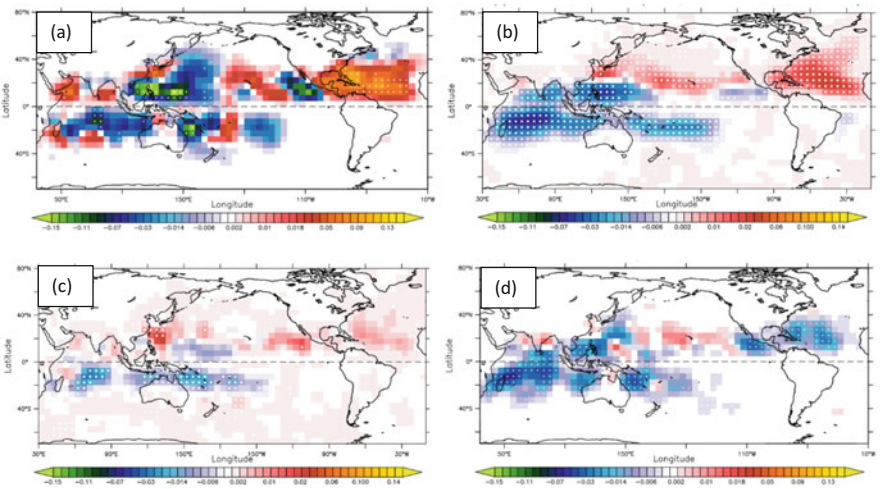

Fig. 1 (**a**) Observed linear trends in TC frequency of occurrence (TCF) for the period 1980–2018 [number per year]. TC positions were counted for each 5° × 5° grid box within the global domain. The total count for each grid box was defined as the TCF. (**b**) As in (**a**), but for the ensemble mean of the large-ensemble experiments using a high-resolution global climate model prescribed with historical time-varying external forcing, such as greenhouse gases, anthropogenic aerosols, ozone, volcanic aerosols, and the solar constant. (**c**) As in (**a**), but for the ensemble mean of the large-ensemble experiments prescribed with time-varying historical volcanic aerosols and the solar constant, while the other forcings were fixed at the 1921 level. (**d**) As in (**a**), but for the experiments in which CO_2 was increased by +1% per year as a boundary condition. (Adapted from Murakami et al. [18]. Licensed under CC BY-NC-ND 4.0)

TCF counted every 6 hours in the observed TC data for every 5° × 5° grid cell. The red shading in Fig. 1a indicates an increasing occurrence of TCs, while the blue shading indicates a decreasing occurrence. The TCF shows significant negative and positive trends, depending on the region, over 1980–2018. For example, the TCF has increased in the NA, central Pacific including Hawaii, and Arabian Sea, whereas it has decreased in the tropical WNP, South Indian Ocean, and along the east coast of the South Pacific, which are all linked to the aforementioned active and inactive TC seasons in the last decade. These recent increases in unprecedented TC seasons in specific regions have aroused public interest regarding the impact of anthropogenic climatic change on TC activity. Although most previous studies have focused on the possible climatic changes in the global TC number, mean TC intensity, and mean precipitation associated with TCs, the climatic changes in regional TCs have not received much attention and have been regarded as relatively more uncertain despite their significant societal importance [1, 13, 14]. This is mainly because of the uncertainty in observations and significant influence of natural variability on TC activity, as discussed in the introduction. In addition, relative to the consistent changes in TC frequency and intensity at the global scale, diverse results have been obtained regarding regional changes in the TC activity projected by many

climate models [14]. Therefore, it has been a challenging issue to estimate any trends in the observed spatial distribution of TCs.

Because of the short duration of the observed record, we primarily rely on climate model simulations to understand forced climate change (e.g., anthropogenic forcing) and internal natural variability (e.g., the PDO, IPO, and AMV). Murakami et al. [18] demonstrated that the observed trends in the spatial distribution of TCs, as shown in Fig. 1a, are attributable to externally forced climate changes that are beyond the influence of internal decadal variability. Figure 1b shows the trend in TCF over the period 1980–2018 as simulated by state-of-the-art climate models forced by natural and anthropogenic external forcings. Note that Murakami et al. [18] conducted the so-called large-ensemble simulations, which is a simulation method that isolates the effect of forced climate change from that of internal natural variability [19]. In short, large-ensemble simulations are historical simulations forced with time-varying external forcing such as greenhouse gases, anthropogenic aerosols, ozone, volcanic aerosols, and the solar radiation constant. Each ensemble member is initialized under a different atmospheric state and oceanic conditions and forward-integrated with prescribed time-varying external forcing. Although atmosphere–ocean coupled models produce a similar evolution of global mean temperature as observed, they generate their own internal variability along with the evolution of the mean state such that each ensemble member exhibits a different phase of internal variability, meaning that some members exhibit a positive PDO while others exhibit a negative PDO, even during the same period. Hence, taking the average of the ensemble members can cancel out the effect of internal variability, and the resultant mean fields can be considered as the response to the external forcing. Figure 1b shows the trend in the ensemble mean TCF fields as simulated in the all-forcing experiments, revealing a similar trend in the spatial pattern of TCF as observed (Fig. 1a). This suggests that the observed trends in the spatial distribution of TCF are attributable to external forcing. In other words, the model results suggest that a climatic change in the global spatial distribution of TCs has already emerged in observations and may in part be attributable to external forcing.

As shown above, it is likely that external forcing has played an important role in the observed change in the global TC distribution since 1980. However, external forcing includes various elements, such as greenhouse gases, anthropogenic aerosols, and volcanic aerosols. Therefore, it is important to quantify the individual contributions that these elements make to the changes in the spatial distribution of TCs. Murakami et al. [18] conducted another set of large-ensemble simulations in which fixed levels of greenhouse gases and aerosols were forced at the 1941 level along with time-varying volcanic forcing and solar radiation to clarify the effect of volcanic and solar activity on the spatial distribution of TCs. Figure 1c shows the trends in TCF simulated by the experiments, in which we can see similar spatial patterns to the observed TCF trends, especially over the Indian Ocean, South Pacific, and NA. Indeed, the simulated spatial pattern of the TCF trend in Fig. 1c indicates that the TC activity in the earlier decades of 1980–2000 was below average for the period in the Northern Hemisphere and above average in the Southern Hemisphere and the sign of the pattern reversed in the later decades of 2001–2018. Associated

with this change, there were two large volcanic eruptions in the Norther Hemisphere in the earlier decades—El Chichón in 1982 and Pinatubo in 1991. Murakami et al. [18] discussed that these two large volcanic eruptions in the Northern Hemisphere might have potentially caused a southward shift in TC genesis locations due to the cooling effect of the Northern Hemisphere and that recovery from this volcanic impact has been taking place since 2000.

Another recent study also reported that mean TC genesis locations could potentially shift southward (northward) after the occurrence of volcanic eruptions in the Northern (Southern) Hemisphere [20]. They argued that a volcanic eruption in one hemisphere would cause asymmetrical hemispheric cooling, which in turn would cause a shift of the Intertropical Convergence Zone (ITCZ) toward the other hemisphere (Fig. 2). This shift of the ITCZ would in turn lead to changes in TC genesis and intensity potential, resulting in an asymmetric anomaly of TC activity between the hemispheres. Therefore, the northward shift in the spatial distribution of TCs, as shown in Fig. 1c, could be partially interpreted as the result of recovery from the surface cooling caused by the two large volcanic eruptions that happened in the

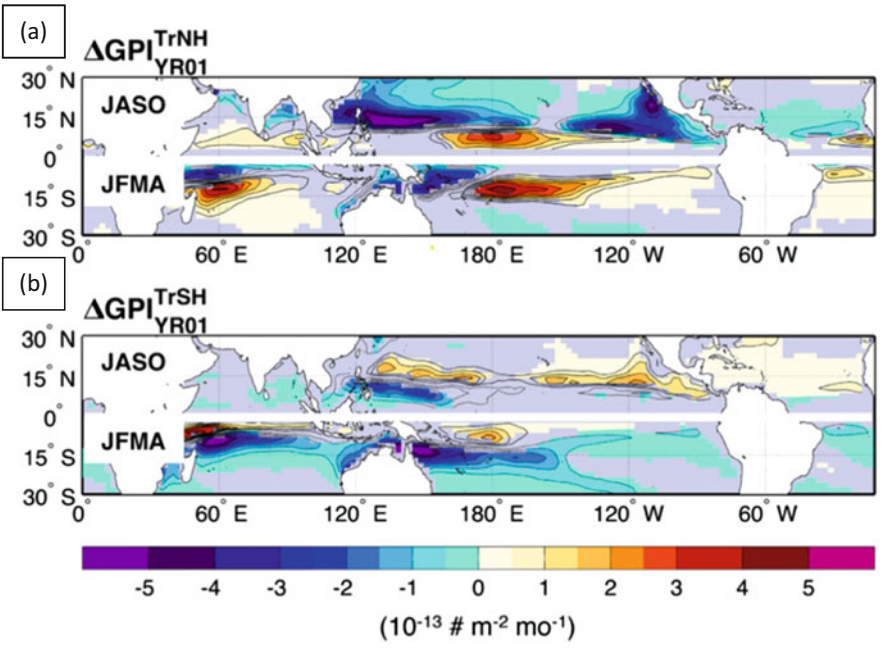

Fig. 2 Changes in TC genesis potential index (GPI) for numerical experiments induced by volcanic eruptions in the Northern Hemisphere (**a**) and Southern Hemisphere (**b**) relative to no-volcano reference simulations for the first storm season in the Northern Hemisphere (July–October) and in the Southern Hemisphere (January–April). GPI is a physically motivated empirical index used to estimate the influence of several large-scale environmental factors on TC genesis frequency. Only values that are significantly different at the 5% level using a *t*-test are shaded. GPI is an index to reflect the degree of TC genesis occurrence that comprises several large-scale factors. (Adapted from Pausata and Camargo [20]. Licensed under CC BY-NC-ND 4.0)

Northern Hemisphere during the 1980s and 1990s. They also revealed, using a dynamical model, that the effect of volcanic eruptions on TC activity lasts for at least 4 years. Evan [21] also reported that the number of TCs in the NA was reduced after the eruptions of El Chichón and Pinatubo and suggested that the reduced TC activity could have been caused by these eruptions. Meanwhile, another study suggested that there is less observed evidence for volcanic events affecting TC activity at the global scale [22]. Indeed, they argued that the reduction in TC activity in the Northern Hemisphere following strong volcanic eruptions cannot be clearly attributable to volcanos, as all the eruptions were coincident with El Niño–Southern Oscillation (ENSO) warm events (i.e., El Niño events). Because El Niño is well known to exert variation in the global distribution of TCs, one cannot immediately conclude that the observed changes in TC activity following volcanic eruptions are purely due to these volcanic eruptions. This debate also stems from the issues discussed in the introduction, i.e., that the length of the reliable observational record is too limited to robustly identify the influence of volcanic events on global TC activity, as well as that there are significant effects of natural internal variability on global TC activity.

To isolate the effect of increases in greenhouse gases on the global distribution of TCs, Murakami et al. [18] conducted another type of experiment in which CO_2 was increased by +1% per year as a boundary condition until the CO_2 level had doubled relative to the level in 1990, while the other external forcings were fixed at their levels in that year. The simulated TCF trend during the period when CO_2 was increased is shown in Fig. 1d, revealing a similar spatial pattern of TCF trends to that observed (Fig. 1a) and that in the all-forcing experiments (Fig. 1b). This indicates that the observed spatial pattern of the global TCF trend during 1980–2018 was probably partially caused by greenhouse gas increases. However, it is interesting to note that there is a different spatial pattern of the TCF trend over the NA, where the model showed a decreasing TCF trend (Fig. 1d), whereas observations showed an increasing one (Fig. 1a). Conversely, the model experiments forced with all external forcings showed an increasing TCF trend in the NA (Fig. 1b). These mixed model results suggest that the observed positive TCF trend in the NA during 1980–2018 may not be related to increases in CO_2, and other external forcings may be involved. Murakami et al. [18] speculated that the increasing TCF over the NA is related to changes in anthropogenic aerosols. Figure 3a shows the simulated and observed number of TCs in the NA, which demonstrates an increasing trend over the period 1980–2018 and a simulated decreasing trend after 2020. Figure 3b shows the specified sulfate over the NA, revealing that the simulated number of TCs is anti-correlated with the prescribed anthropogenic aerosols during 1960–2020, insofar as the simulated number of TCs is lower around 1980 when sulfate aerosols over the NA are higher, whereas the simulated number of TCs in the NA shows an increasing trend between 1980 and 2020 when anthropogenic aerosols show a decreasing trend over that period. Why, then, did the increase (decrease) in anthropogenic aerosols inhibit (stimulate) the TC activity in the NA? Particulate pollution and other aerosols affect clouds and precipitation processes and reflect sunlight away from the earth, causing regional cooling of the oceans such that the

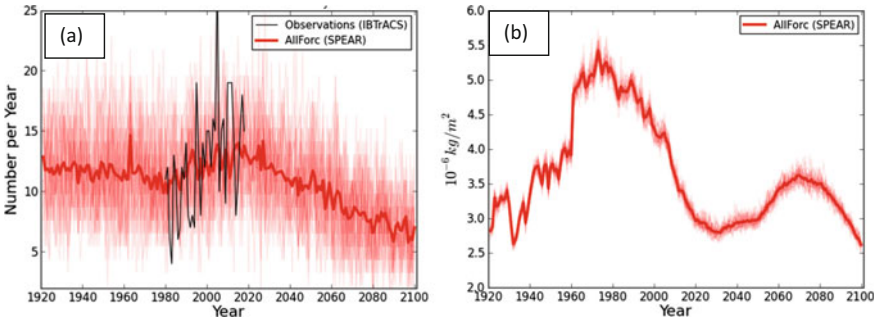

Fig. 3 Time series of observed and simulated TC numbers and sulfate aerosols in the North Atlantic by Murakami et al. [18]. (**a**) Annual TC number in the North Atlantic [units: number per year]. (**b**) Annual mean sulfate aerosols over the North Atlantic Ocean [5°N–45°N, 10°W–90°W; units: 10^{-6} kg m^2]. The black line in (**a**) is from observations. The thin red lines in (**a**) and (**b**) are the TC numbers and sulfate aerosols, respectively, simulated by the 30-member large-ensemble simulations with all forcing by a dynamical model, while the thick red line is the ensemble mean. (Adapted from Murakami et al. [18]. Licensed under CC BY-NC-ND 4.0)

large-scale oceanic condition is unfavorable for TC activity. In line with their technological development, European countries and the USA suppressed emissions of manmade aerosols from the early 1980s, which led to a surface ocean warming in the NA in the model simulations. This in turn probably contributed to the observed increased activity of TCs over the NA during the period 1980–2020. This increased TC activity in the NA due to diminished anthropogenic aerosols was also studied by Dunstone et al. [23] and Sobel et al. [24]. Despite the projected low level of anthropogenic aerosols after 2020 (Fig. 3b), the projected number of TCs in the NA continues to decrease in the model simulations (Fig. 3a). This suggests that the effect of greenhouse gases will dominate in the future in relation to reduced numbers of TCs in the NA in the model simulations.

3 Changing TC Tracks Near Coastal Regions

In the previous section, the observed changes in the global distribution of TCs over the past 40 years were discussed. However, the most important and relevant topic for society is whether TCs are tending to approach coastal regions more frequently. Kossin et al. [25] reported poleward migration of the mean locations where observed TCs reached their lifetime maximum intensity (LMI) in the past 40 years. However, this poleward migration of the LMI may not directly indicate an increasing risk of coastal TCs because these locations are commonly over the open oceans and too far from coastal regions to generate any impacts on human society. Therefore, quantifying the changes in coastal TC activity, landfall frequency, and TCs over land is more central to estimating and mitigating the risks of storm-related damage in the future.

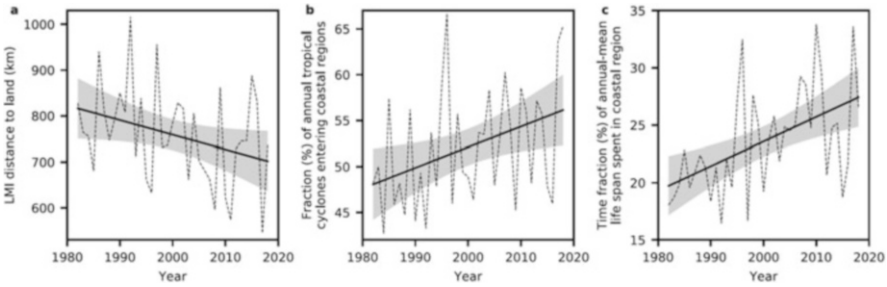

Fig. 4 Landward migration of global TC activity. (**a**) Time series of the annual mean distance between land and locations of lifetime maximum intensity (LMI) [km]. (**b**) As in (**a**), but for the fraction of annual TCs entering coastal regions [%]. (**c**) As in (**a**), but for the time fraction of the annual mean lifespan spent in coastal regions [%]. The dashed lines show the historical data. The solid lines show the linear trends. The shading represents the 95% confidence interval of the linear trend. (Adapted from Wang and Toumi [26]. @Science. Used with permission)

In addition to poleward migration of the LMI, Wang and Toumi [26] reported an increasing trend in the frequency of coastal TCs worldwide over the period 1982–2018. Figure 4a shows the observed trend in the mean distance between the land surface and TC locations. The data indicate that the annual mean distance of the LMI to the nearest land mass shows a statistically significant decreasing trend of around −32 km per decade across the globe. Figure 4b indicates that the annual fraction of TCs entering global coastal regions, defined as the offshore area with a distance to the nearest land mass of less than 200 km, shows a robust increase of around +2.2% per decade. Figure 4c indicates that there is a positive trend in the annual mean fraction of their lifetime that TCs spend in coastal regions, at a statistically significant rate of around +2.1% per decade. Table 1 also shows the observed changes in mean TC locations between the periods 1982–1999 and 2000–2018, revealing that, across the world's basins, these have been migrating not only poleward but also westward. Considering the global distribution of land and sea, this westward shift of TC locations is expected to lead to a more frequent occurrence of TCs in coastal regions. Moreover, Table 1 shows that the magnitude of the mean shift in TC locations is larger in the zonal than the meridional direction. Specifically, mean TC locations have been shifting westward in the WNP, East Pacific, and Indian Ocean. These basins accounted for 75% of the world's TCs during 1982–2018, which explains the global mean westward shift in TCs and indicates a greater risk of storm-related damage for society. TC locations are primarily determined by the environmental steering flow, but also the locations of TC genesis. Wang and Toumi [26] revealed a significant enhancement in the westward trend in steering flows at the global scale (Table 1). They also found greater reductions in vertical wind shear in western than eastern domains across all of the world's basins, indicating more favorable large-scale conditions for TC genesis and propagation in the western domains than in the eastern domains.

Related to the findings of Wang and Toumi [26], Yamaguchi and Maeda [27] also reported an increasing number of TCs approaching Tokyo since 1980

Table 1 Changes in the observed mean TC locations (units: degree) and deep-layer zonal steering flow (units: m s^{-1}) between the periods 2000–2018 and 1982–1999

	Global	NHEM	SHEM	WPAC	EPAC	NATL	NIO	SIO	SPAC
Westward	**+0.8 ± 0.2**	**+1.0 ± 0.3**	**+0.4 ± 0.3**	**+1.6 ± 0.4**	**+1.3 ± 0.7**	–0.1 ± 0.5	**+2.7 ± 0.4**	**+1.4 ± 0.5**	**–1.6 ± 0.6**
Poleward	**+0.3 ± 0.1**	**+0.2 ± 0.1**	**+0.6 ± 0.2**	**+0.5 ± 0.2**	**+0.4 ± 0.2**	**–0.3 ± 0.3**	**–0.8 ± 0.3**	**+0.6 ± 0.2**	**+0.5 ± 0.3**
Steering	**+0.3 ± 0.3**	+0.2 ± 0.3	+0.4 ± 0.6	**+0.4 ± 0.4**	**+0.4 ± 0.3**	+0.1 ± 0.3	–0.1 ± 0.3	+0.3 ± 0.5	+0.5 ± 0.7

The steering flow is calculated with reanalysis data. Statistical significance at the 95% confidence interval is indicated in bold. The differences are calculated globally, in the hemispheres (*NHEM* Northern Hemisphere; *SHEM* Southern Hemisphere) and in the six individual basins (*NATL* North Atlantic; *WPAC* Western North Pacific; *EPAC* East Pacific; *NIO* North Indian Ocean; *SIO* South Indian Ocean; *SPAC* South Pacific). Adapted from Wang and Toumi [26]. @Science. Used with permission

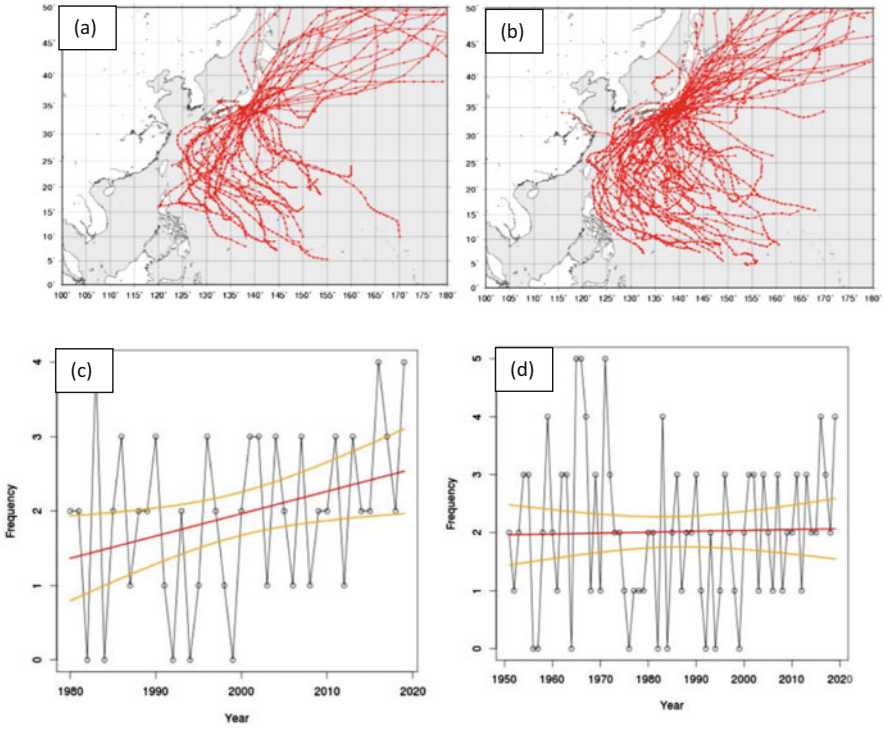

Fig. 5 All TC tracks that approached Tokyo in (**a**) 1980–1999 and (**b**) 2000–2019, showing increasing numbers in the latest decades. Time series of the number of TCs that approached Tokyo over (**c**) 40 years from 1980 to 2019 and (**d**) 69 years from 1951 to 2019. The linear regression and the 95% confidence interval around the linear regression line are shown in red and orange, respectively. (Adapted from Yamaguchi and Maeda [27]. Used as open access)

(Fig. 5). Figure 5a–c indicates that the number of TCs approaching the southern coast of Japan, including Tokyo, has increased over the last 40 years. Yamaguchi and Maeda [27] indicated that, in the most recent decades relative to the decades before, the subtropical high had strengthened and the westerly jet had weakened, leading to a more conducive large-scale environment for TCs approaching Tokyo. However, when the trend analysis was extended to the pre-satellite era (e.g., 1951–2019, Fig. 5d), there was no significant trend in the number of TCs approaching Tokyo. Note that, relative to TC data over the open oceans, TC records near land before the satellite era could be more reliable because the Japan Meteorological Agency has been recording in situ observations and statistics on the number of TCs approaching Japan since 1951. Given the steady number of TCs near Tokyo over the longer period of 1951–2019, Yamaguchi and Maeda [27] speculated that, rather than being related to anthropogenic climate change, the increasing number of TCs near Tokyo over the recent period of 1980–2019 may instead be related to natural decadal variability, such as the PDO.

On the other hand, Wang and Toumi [26] showed that the observed trend in the westered shift in TC locations was still significant even after statistically removing the influence of the PDO. Thus, it is still uncertain as to the extent of the roles played by natural decadal variability and anthropogenic climate change as identified by Wang and Toumi [26] and Yamaguchi and Maeda [27], because both studies were based on observational data analysis. Further studies using climate models may help improve our understanding of the cause of the shifts in mean TC locations.

4 Slower Decay of Landfalling TCs

The source of energy for a TC is the release of latent heat through the evaporation of water from the ocean surface. Therefore, once a TC makes landfall, it disconnects from its energy source and starts to decay. In this respect, it is expected that a TC will last longer over the land surface if the initial TC intensity at landfall is stronger, and a recent study by Li and Chakraborty [28] reported a tendency in recent decades for hurricanes over the NA to be doing just that, spending more of their lifetime farther inland. They analyzed the 71 hurricanes over the NA that made landfall during the period 1967–2018 (Fig. 6a). TC intensity (V) decays exponentially after making landfall, as follows:

$$V(t) = V(0)e^{-t/\tau}, \tag{1}$$

where t is the time past landfall and τ is the decay timescale that characterizes the rate of decay. The larger the τ, the slower the decay and therefore the stronger the hurricane. Figure 6b shows a histogram of τ for the periods 1967–1992 and 1993–2018, revealing larger τ over the latter period, meaning slower decay over land in recent decades. There is a high correlation between the interannual variation in τ and the mean sea surface temperature (SST) over the tropical NA (correlation coefficient = 0.73) (Fig. 6c), indicating a substantial effect of ocean warming on the slower decay of landfalling TCs. It is interesting to note that it is not the initial TC intensity that determines τ but the "storm moisture." Storm moisture is defined as the total moisture that a TC holds at the time of landfall. Li and Chakraborty [28] conducted numerical simulations using a three-dimensional, non-hydrostatic, non-linear, time-dependent computational model that had been used to study the dynamics of idealized hurricanes. They simulated four TCs under different SST conditions. Although the simulated TC intensity at landfall was set at 60 ms^{-1} and identical for all TCs, the τ was larger when the SST was higher (Figs. 7a, b). They also conducted additional "dry experiments" in which moisture was removed at the time of landfall, and the results showed no difference in TC intensity and τ among the four TCs after landfall (plus symbols in Fig. 7a), indicating that it is the total moisture at landfall that causes the difference in τ. This means that warmer SST can enable a TC to hold more moisture over the ocean (i.e., the Clausius–Clapeyron relation), which then makes the TC survive longer over land. Therefore, it is likely that global warming will make TCs last longer over the land surface. Li and Chakraborty [28] also

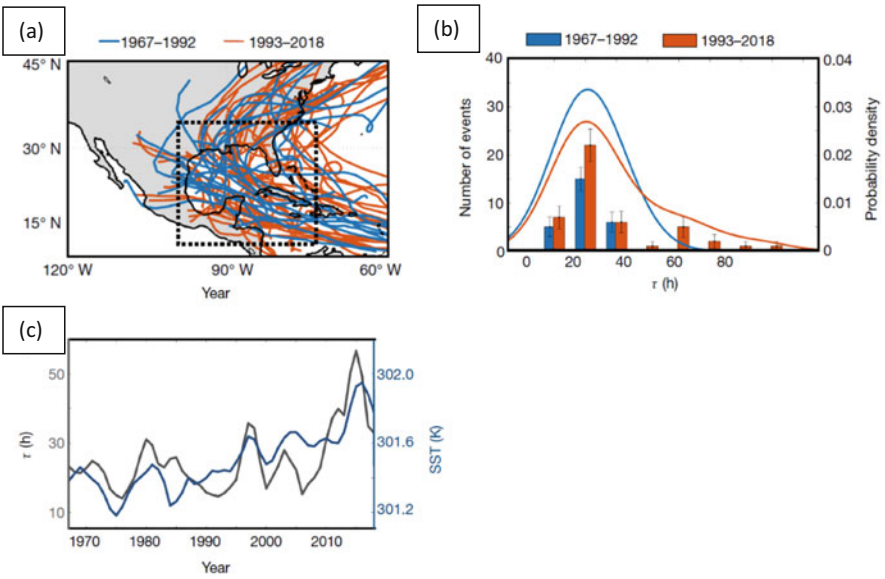

Fig. 6 North Atlantic landfalling hurricanes and the effect of sea surface temperature (SST) on the decay of hurricanes. The 71 landfalling hurricane events during 1967–2018 were analyzed. (**a**) Observed hurricane tracks during 1967–1992 (blue) and 1993–2018 (red). (**b**) Histogram and probability density of τ, which is a measure of the mean duration of landfalling TCs. The average τ increases from 21.2 ± 1.3 h (1967–1992, 26 events) to 28.4 ± 2.4 h (1993–2018, 45 events). The error bars in the histogram are computed using the bootstrap sampling method and correspond to ±1 standard deviation. (**c**) Interannual variation of τ (black) and SST over the tropical Atlantic (10–35°N, 75–100°W). (Adapted from Li and Chakraborty [28]. Used with permission from Springer Nature)

indicated that an eastward shift in TC tracks in the NA may be related to the increasing τ. Although the reason is unclear, the decay in the northeast USA is climatologically slower than the decay in the southeast USA. Overall, there is a significant positive trend in the mean duration of TCs staying over the land surface, and this trend may be related to the surface ocean warming over the tropical NA. However, it is still not clear if the observed trends in duration and SSTs over the period 1967–2018 were purely due to global warming induced by increased CO_2, as previous studies have also indicated that SST warming has been influenced by the decreasing trend in anthropogenic aerosols and/or multidecadal natural variability [18].

An increasing trend in the duration of TCs staying over land has also been observed in the WNP. Chen et al. [29] documented that there was an increasing trend in the annual average overland duration of a TC over mainland China during the period 1975–2009. Liu et al. [30] extended the analysis using the observed data up to 2018 and reported that TCs have shown a tendency over the past 40 years to last longer after making landfall over mainland China (Fig. 8). Although the frequency of TCs making landfall over mainland China shows no apparent

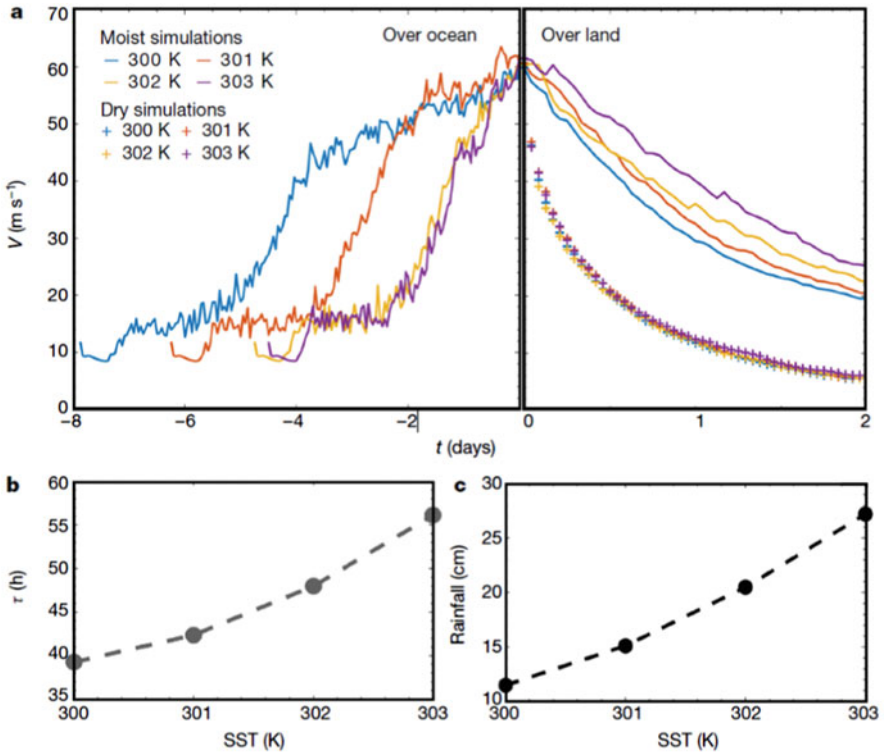

Fig. 7 Effect of sea surface temperature (SST) on the decay of simulated landfalling hurricanes. Four different hurricanes were simulated using a dynamical model prescribed with different SSTs. (**a**) Maximum wind speed (V) versus time (t) relative to landfalling time. For $t < 0$, the TCs develop over warm oceans. The different colors represent different SSTs. At $t = 0$, the hurricanes make landfall with $V \approx 60$ m s^{-1}. The solid lines correspond to the moist simulations and the plus symbols to the dry simulations. (**b**) τ versus SST. (**c**) Rainfall versus SST. (Adapted from Li and Chakraborty [28]. Used with permission from Springer Nature)

increasing or decreasing trend over the period 1980–2018 (Fig. 8a), there is an increasing trend in the mean duration of TCs over land (Fig. 8b), as well as an increasing trend in the mean TC intensity at landfall (Fig. 8c) and a weak increasing trend in the mean TC translation speed over land (Fig. 8d). Liu et al. [30] attributed the increasing trend in mean TC duration over land to an increasing trend in the traveling distance over land from the coastline and the northward shift in TC tracks over mainland China. Moreover, Liu et al. [30] highlighted that the decrease in the intensity of the weakening rate after landfall must be the factor responsible for the longer duration of TCs over land, which is consistent with the findings of Li and Chakraborty [28]. Liu et al. [30] reported that these trends in the mean TC duration over land could be linked to the increasing SSTs in the coastal region of mainland China, which provide favorable conditions for increasing the TC intensity prior to landfall. In addition, increases in land-surface temperature and soil moisture and a

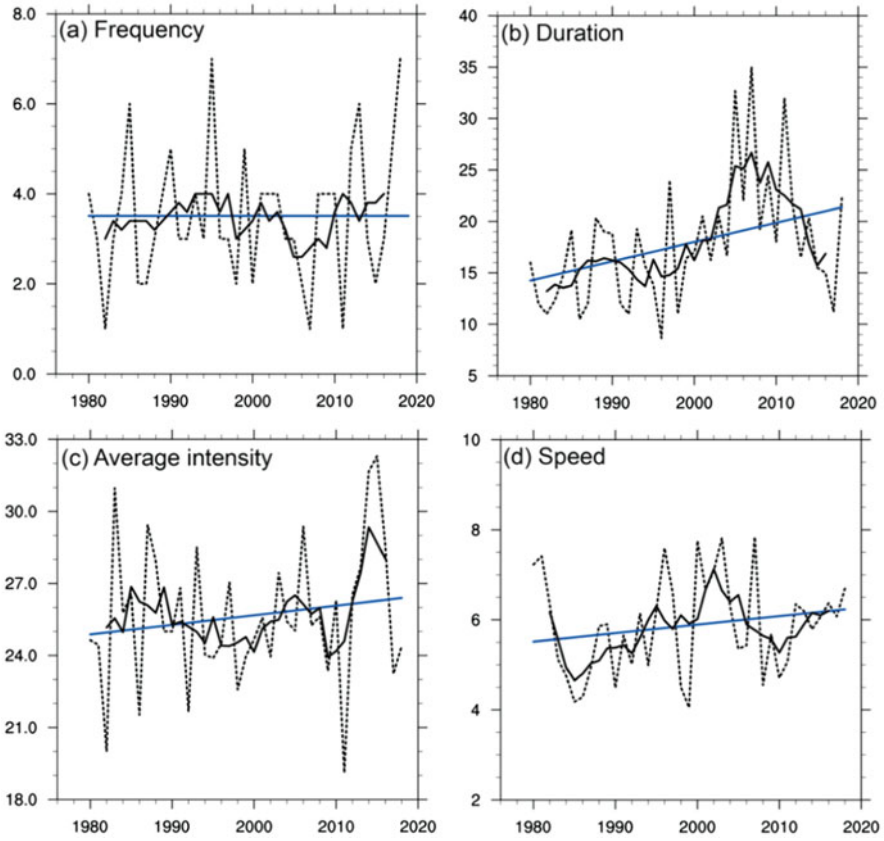

Fig. 8 Time series of the (**a**) number of landfalling TCs over mainland China, (**b**) average TC duration [h], (**c**) average intensity [m s^{-1}], and (**d**) average translation speed [m s^{-1}] after landfall in the peak TC season of July–October during 1980–2018. Thick black lines denote the 5-year running average, and the blue lines indicate the corresponding linear trends. (Adapted from Liu et al. [30]. @American Meteorological Society. Used with permission)

lower tropospheric humidity are the thermodynamic conditions favorable for increasing the mean overland duration of TCs after landfall. As in Li and Chakraborty [28], it is not clear if the trends are due to anthropogenic climate change or natural internal variability. Indeed, previous studies have shown the importance of the IPO, which is an apparently internal variability at the decadal time scale that manifests as a low-frequency El Niño-like pattern of climate variability for the SSTs over the WNP. A recent negative phase of the IPO (1998–2013) was characterized by a La Niña-like SST anomaly pattern in the tropical Pacific with more significant warming in the northwest and southwest Pacific that also led to increasing SSTs near the coast of mainland China. The IPO changed sign around 2013 to a positive phase. Indeed, the time series of the mean duration of TCs over land after landfall appears to

be correlated with the IPO (Fig. 8b). Further studies using climate models will help improve our understanding of the cause of these observed trends.

5 Pseudo-global Warming and Hindcast Attribution Experiments

As indicated in the previous section, there are some significant observed trends in TC activity that might be related to anthropogenic climate changes. However, it is challenging to identify the causes of these trends just by analyzing observed datasets, and we therefore rely heavily on numerical experiments for this purpose. The large-ensemble-experiment method, which was introduced in the previous section, is useful to explore whether any observed trends in TC activity were likely related to anthropogenic climate changes in the past. However, there is a large gap between scientific and public interests; the public is far more interested in specific TCs and/or TC seasons rather than the mean changes in basin-scale or global TC activity. Specifically, the major public interest is the relevance of any climatic change to the occurrence of individual TCs or TC seasons. For example, there was strong public interest regarding the extent to which anthropogenic climate change contributed to the occurrence of extreme TCs such as Hurricane Katrina in 2005 and/or an extreme hurricane season, such as in 2020, in which a record 30 named storms were observed in the NA. However, scientific knowledge is far too limited to answer specific questions such as these, and this is mainly because the occurrence of individual TCs and extreme hurricane seasons is substantially chaotic in general (i.e., small signal-to-noise ratio). Thus, it is challenging to quantify the effect of climatic changes on individual TCs and hurricane seasons, specifically in terms of their probability of occurrence. Despite this challenge, there are recent studies that have attempted, using high-resolution models, to attribute some aspects of individual extreme events in the form of individual TCs or hurricane seasons to anthropogenic forcing. A detailed review of this methodology is available in Wehner et al. [31], so only a brief introduction and summary of recent studies are provided here, as follows:

First, there are recent studies that have applied the so-called "pseudo-global warming" experiments to individual storms to quantify the effect of anthropogenic warming on their storm intensity [31–33]. This type of experiment is also called "hindcast attribution." Unlike modeling studies using global models as introduced in the previous section, these studies utilized regional models. Generally, regional models need lateral boundary conditions as well as surface boundary and initial conditions. A pair of experiments is used for pseudo-global warming experiments. The first is the control experiment in which an actual TC is simulated given realistic initial, lateral, and surface boundary conditions derived from observations or reanalysis data. This control experiment is the same as dynamical model simulations applied in weather forecasts in which realistic simulations of TC tracks and intensity relative to observations are required for the following counterfactual experiment, which is the second experiment of the pair. In these experiments, expected

perturbations due to global warming are removed from (or added to) the lateral boundary and initial conditions used in the control experiment. Therefore, if a reanalysis dataset is used for the boundary condition in the control experiment, then the only additional counterfactual experiment conducted is one in which the perturbations are added (removed) to (from) the original lateral boundary conditions for each time step. The perturbations are generally derived from climate model simulations by global models. The common variables used to remove or add the perturbations are thermodynamic parameters such as atmospheric temperature and specific humidity. For example, suppose there is a present-day climate simulation using a global model as well as a pre-industrial climate simulation in which greenhouse gases are fixed at the pre-industrial level. The perturbations are defined as the differences in the simulated mean large-scale parameters between the present-day and pre-industrial simulations. These perturbations are removed from the lateral boundary conditions used for the control experiment so that the same TC can be simulated under the same synoptic-scale conditions but with the mean pre-industrial climate. There are a few advantages to using regional models over global models. For example, regional models can save on computational resource. Moreover, some of these models apply a non-hydrostatic framework so that high-resolution configurations with cloud systems being directly simulated can result in more realistic simulations of TC intensity. Such pseudo-global warming experiments are used to estimate how much anthropogenic warming contributed to changes in TC intensity for a specific TC in terms of maximum wind speed or precipitation. Therefore, this method cannot establish whether anthropogenic warming might have caused a change in occurrence of the TC itself because the experiments are conducted from the initial conditions under which the targeted TC already existed. In addition, a disadvantage of the method is that it assumes the TC track will not change under a different climate. This assumption is made because the estimated thermodynamic effect of anthropogenic warming on TC intensity can be estimated only when the TC track is the same between the control and counterfactual experiments. Otherwise, the simulated changes in TC intensity could be mixed up due to anthropogenic warming and/or simply the differences in the simulated TC tracks. Therefore, perturbations are not added to dynamical parameters such as the zonal and meridional winds because these perturbations can cause changes in TC tracks. Given that many previous studies using global models have suggested that changing the climate can also alter the mean TC tracks [34, 35], this assumption of unchanging TC tracks under different climates may not be justified and may not fully explain the effect of anthropogenic warming on individual TC activities. It is also expected that wind fields are tightly linked to temperature fields under the thermal wind relation, meaning altered temperature and humidity fields may not be balanced with wind fields.

Patricola and Wehner [32] applied pseudo-global warming experiments to 15 major TC events that occurred in the NA and Pacific using the Weather Research and Forecasting (WRF) regional climate model developed by the National Center for Atmospheric Research. They conducted counterfactual pre-industrial experiments as well as future experiments under the Representative Concentration Pathway (RCP) 4.5, 6.0, and 8.5 scenarios for each storm. Figure 9 and Table 2 show the simulated

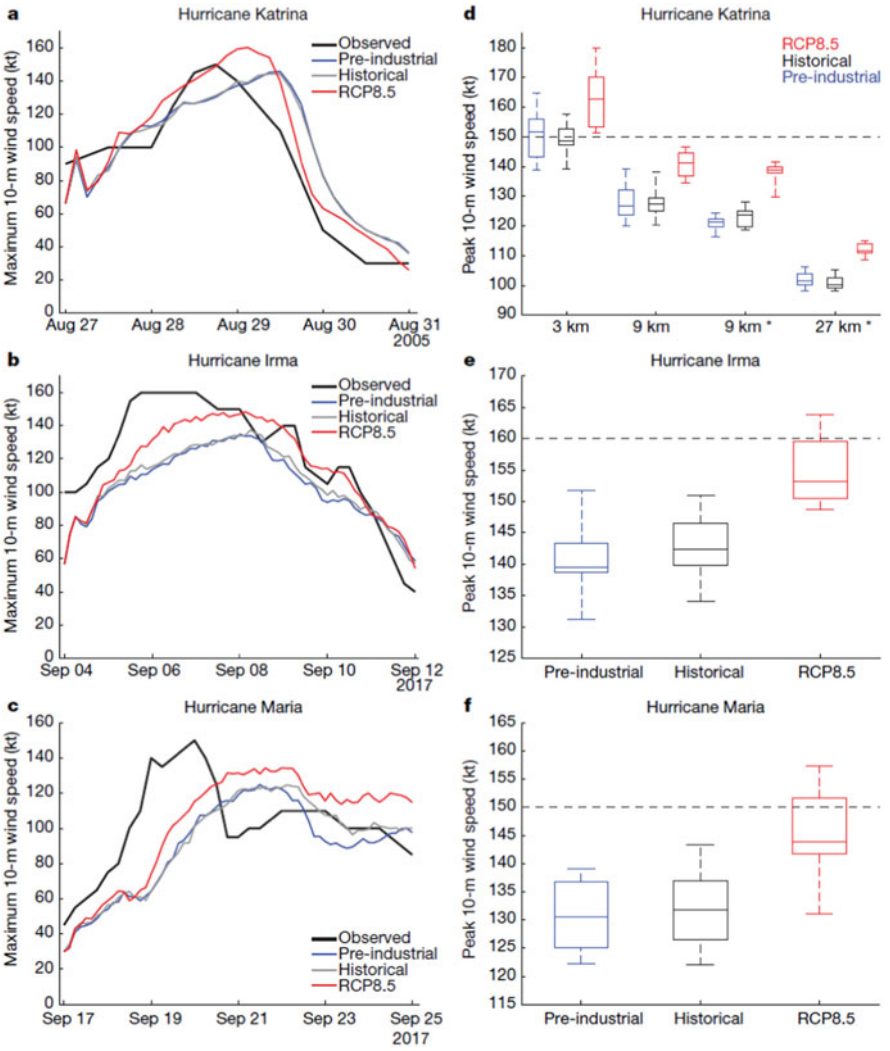

Fig. 9 Time series and boxplots of TC maximum 10-m wind speed. (**a**–**c**) Time series of maximum 10-m wind speed [kt] from observations (black) and the ensemble mean of the pre-industrial (blue), historical (gray), and RCP8.5 (red) simulations of Hurricane (**a**) Katrina at 3-km resolution, (**b**) Irma at 4.5-km resolution, and (**c**) Maria at 4.5-km resolution. (**d**–**f**) Boxplots of peak 10-m wind speed [kt] from the 10-member ensemble of pre-industrial (blue), historical (black), and RCP8.5 (red) simulations of (**d**) Hurricane Katrina at 3-km, 9-km (with and without convective parameterization), and 27-km resolution, and Hurricane (**e**) Irma and (**f**) Maria at 4.5-km resolution. The center line denotes the median; box limits denote the lower and upper quartiles; and whiskers denote the maximum and minimum. The observed peak intensity is marked with a horizontal black line. Simulations that used convective parameterization are denoted by an asterisk. (Adapted from Patricola and Wehner [32]. Used with permission from Springer Nature)

Table 2 TC peak 10-m wind speed simulated by the pseudo-global warming experiments conducted by Patricola and Wehner [32]

Basin	Tropical cyclone	Resolution	Historical minus pre-industrial	RCP4.5 minus historical	RCP6.0 minus historical	RCP8.5 minus historical	Historical	Observed
Atlantic	Katrina	27 km (P)	–1.0			11.0**	101	150
		9 km (P)	2.0			15.2**	123	150
		9 km	–0.5			13.5**	127	150
		3 km	–2.4			13.7**	149	150
		4.5 km		6.0**	8.5**	13.8**	142	150
	Irma	4.5 km	–1.9	7.3**	10.4**	12.4**	143	160
	Maria	4.5 km	–1.5	7.5**	10.9**	12.9**	132	150
	Andrew	4.5 km		–3.3	–2.4	–1.7	118	150
	Bob	4.5 km		–6.1**	–2.4*	2.1	78	100
	Floyd	4.5 km		11.2**	13.5**	X	118	135
	Gilbert	4.5 km		18.0**	18.6**	28.8**	109	160
	Ike	4.5 km		12.8**	14.1**	18.0**	127	125
	Matthew	4.5 km		10.6**	11.1**	15.8**	123	145
Eastern Pacific	Iniki	4.5 km		–0.4	–3.9	4.6*	114	125
Northwest Pacific	Haiyan	4.5 km		6.7**	3.8	12.3**	124	170

(continued)

Table 2 (continued)

Basin	Tropical cyclone	Resolution	Historical minus pre-industrial	RCP4.5 minus historical	RCP6.0 minus historical	RCP8.5 minus historical	Historical	Observed
	Morakot	4.5 km		0.5	X	X	71	80
	Songda	4.5 km		10.4**	5.5**	X	109	125
South Pacific	Yasi	4.5 km		11.2**	13.7**	18.9**	95	135
Southwest Indian	Gafilo	4.5 km		8.6**	8.8**	16.8**	110	140

The mean difference in TC peak 10-m wind speed is given (in knots) between the historical and pre-industrial simulations and between the RCP4.5, RCP6.0, and RCP8.5 simulations and the historical simulation, along with the TC peak 10-m wind speed from observations and the ensemble-mean historical simulation. Cases with substantial differences between simulated and observed TC tracks are denoted "X" and simulations that were not performed are blank. A single (double) asterisk indicates statistical significance at the 10% (5%) level. Simulations that used convective parameterization are denoted 'P'. Adapted from Patricola and Wehner [32]. Used with permission from Springer Nature

TC intensity. They first tested the dependency of the model resolution on the results. By using the four different horizontal resolutions of the WRF model (i.e., a 27, 9, 3, and 4.5 km mesh), they applied the pseudo-global warming experiments to Hurricane Katrina (Table 2). They found that all resolutions generally showed an increase in maximum wind speed by around +11–13.8 knots under the RCP8.5 scenario relative to the present-day climate, revealing that the difference in model resolution did not severely alter the results. They also conducted the experiments with and without cumulus parameterization in the regional model, and the results showed minimum uncertainty for the sign of the projected changes in TC maximum wind speed and rainfall. These findings instill greater confidence in projections of TCs by models with parameterized convection and a resolution fine enough to include TCs. Overall, they showed that future anthropogenic warming would robustly increase the TC maximum wind speed and rainfall of 11 of 13 intense TCs. On the other hand, they also showed that the climate change between the present-day and pre-industrial conditions might have enhanced the average and extreme rainfall of hurricanes Katrina, Irma, and Maria, but did not significantly change the TC maximum wind speed.

Similar pseudo-global warming experiments were conducted by Reed et al. [33] for Hurricane Florence. Unlike the study by Patricola et al. [32], Reed et al. [33] utilized a high-resolution global atmospheric model (the Community Atmosphere Model, version 5) with a variable resolution configuration involving 30 vertical levels, a base horizontal grid spacing of 110 km, and a refined region over the NA with a grid spacing of roughly 28 km. The model simulations were initialized with the atmospheric and ocean surface analysis derived from the National Oceanic and Atmospheric Administration's Global Forecast System. The model was initialized every 12 hours starting from 9 September at 12Z to 12 September at 00Z. There were 96 ensemble members in total for the pseudo-global warming and control experiments. The control experiment was called the "Actual" experiment, which involved hindcast experiments forced with the observed conditions (i.e., the actual world). The counterfactual experiment was referred to as "Counterfactual," in which the estimated signal of climate change was removed from the initial conditions for the three-dimensional air temperature, specific humidity, and two-dimensional SSTs. The signal was preliminarily computed from long-term climate experiments. Also, in the Counterfactual experiments, the greenhouse gas concentrations, solar radiation conditions, ozone concentrations, and aerosol concentrations were all set to their levels in the year 1850 to mimic the pre-industrial climate. Figure 10a shows the simulated and observed storm track for Hurricane Florence initialized at 0Z on 11 September, in which the simulated tracks by the Actual (red) and Counterfactual (blue) experiments resemble the observed tracks. Figure 10b shows the simulated total accumulated rainfall over land, revealing significant increases in total rainfall over land by the Actual experiments compared to the Counterfactual experiments. This suggests that the severe rainfall over land during the landfall of Hurricane Florence is attributable to the changes in anthropogenic climate change. Overall, Reed et al. [33] concluded the following from their pseudo-global warming experiments:

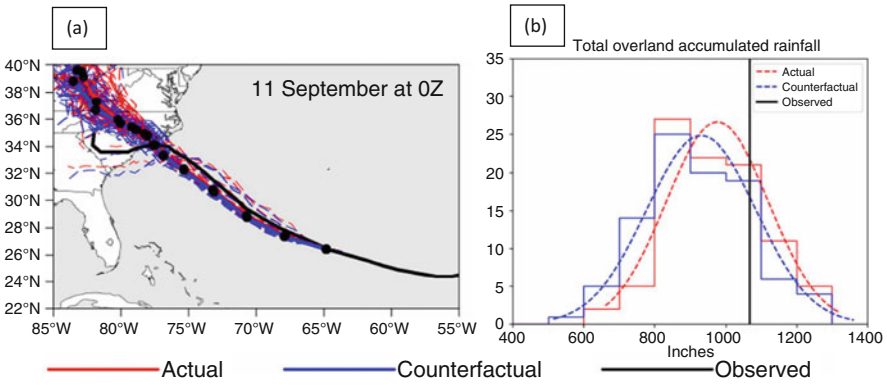

Fig. 10 (**a**) Observed and simulated storm tracks by Reed et al. [33]. Model simulated TC tracks of the 7-day Actual (red) and Counterfactual (blue) forecasts initialized on 00Z, 11 September 2018. Solid lines are the ensemble mean, and dashed lines are the individual ensemble members. Black lines are the observed track. Black dots on the ensemble mean tracks represent the locations of the hurricane center at 12-hour intervals. (**b**) Simulated changes in total accumulated rainfall within 200 km and 48 hours of the model landfall for the Actual (red) and Counterfactual (blue) 11 September 00Z ensembles. Dashed lines are Gaussian fits to the data. Only 96 ensemble members that made landfall within 200 km of the observed landfall location were included. The observations are marked with the vertical black line. (Adapted from Reed et al. [33]. Licensed under CC BY-NC-ND 4.0)

1. Hurricane Florence would have been slightly more intense for a longer portion of the forecast period due to climate change.
2. The rainfall amounts of Hurricane Florence over the Carolinas would have increased by over 50% due to climate change and were linked to warmer SSTs and available moisture in the atmosphere.
3. Hurricane Florence would have been about 80 km larger because of the effect of climate change on the large-scale environment around the storm.

Note that Reed et al. [33] conducted these experiments in real time when Hurricane Florence was about to make landfall. They made these statements 2 days before the landfall of Hurricane Florence. This "real-time attribution" was made based on simulations using the hindcast attribution method before the real hurricane made landfall, but was expected to make landfall. This real-time attribution approach is useful for providing timely information for the public regarding the relationship between concurrent TCs and climate changes.

6 Attribution Experiments Based on Seasonal Predictions

Event attribution has also been applied to unprecedented TC seasons to identify the physical mechanisms underpinning their occurrence in relation to climate changes [16, 36, 37]. For example, Murakami et al. [36] studied the active MH season in

2017 in the NA using a high-resolution seasonal prediction model. The 2017 hurricane season in the NA was highly active, with six MHs, including three that made landfall (hurricanes Harvey, Irma, and Maria; Fig. 11a). These MHs were largely concentrated in the tropical NA (Fig. 11b). Given the mean number of MHs in the NA is around 1 per year, this unprecedented event of Atlantic MHs attracted

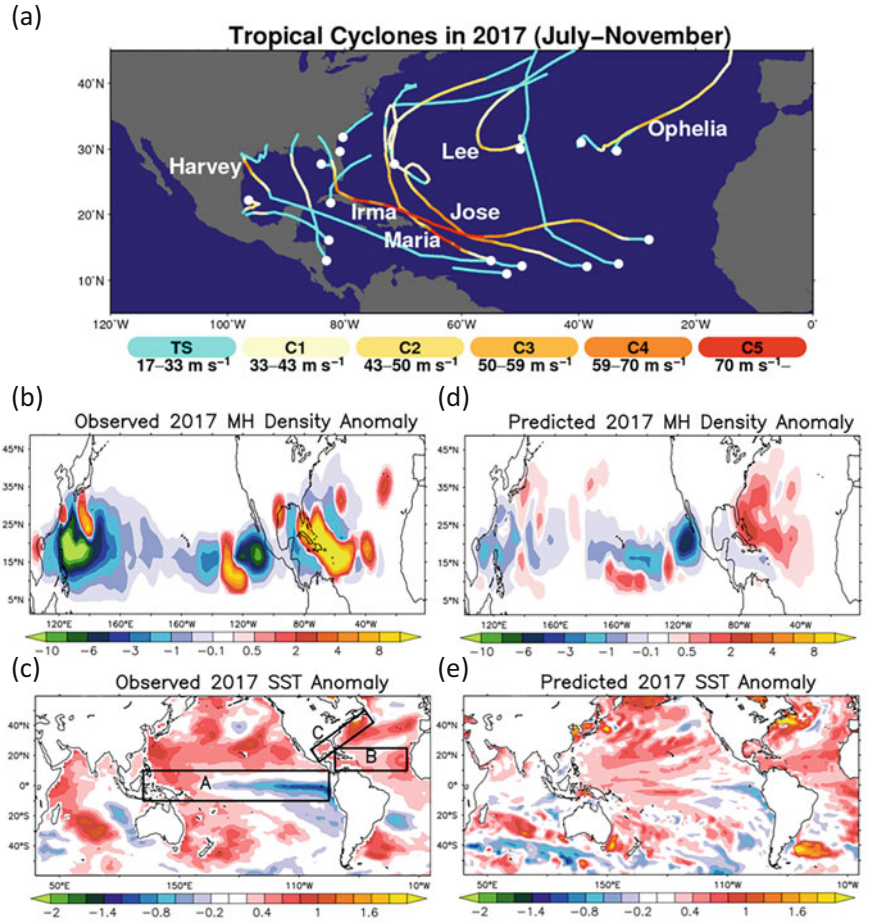

Fig. 11 (**a**) Observed tropical cyclones during the hurricane season in 2017. Storm tracks are colored according to the intensities of the storms, as categorized by the Saffir–Simpson hurricane wind scale (TS, tropical storm; C1–C5, category 1 to category 5 hurricanes). Labeled storms denote major hurricanes (MHs). (**b**) Observed MH density anomaly in the 2017 hurricane season relative to the mean of 1980–2017 (number per 2.5° × 2.5° grid box per season). (**c**) Observed sea surface temperature (SST) anomaly (units: K) in the 2017 hurricane season relative to the mean of the period 1982–2012. The black frames are the possible key regions for the unusually high MH activity in 2017. (**d**, **e**) As in (**b**, **c**) but for the ensemble mean of real-time seasonal predictions from 1 July 2017 initials predicted by the HiFLOR model developed by the Geophysical Fluid Dynamic Laboratory. (Adapted from Murakami et al. [36]. @Science. Used with the author's copyright)

considerable attention throughout the scientific community and broader society, not only in terms of the causes but also whether anthropogenic warming played a role. Several large-scale factors might have caused the active MH season. As shown in the SST anomaly in 2017 (Fig. 11c), the summer of 2017 was characterized by a developing moderate La Niña ("A" in Fig. 11c). It is well known that during a La Niña summer, hurricanes are generally more active over the NA due to a weakening vertical wind shear in the tropical Atlantic. It is also clear that the surface ocean was substantially warmer in the tropical NA (region "B" in Fig. 11c), which is a region where many MHs generate [i.e., the main developing region (MDR)]. In addition, a substantial positive SST anomaly was also observed over the coastal regions (region "C" in Fig. 11c). It is expected that TCs obtain more energy from warmer oceans and then further develop into MHs. This particularly active MH season in 2017 and the associated SSTs were predicted well in the real-time seasonal prediction starting from 1 July 2017 using a high-resolution global coupled model (Fig. 11d). To clarify the relative importance of the SST anomalies over the three key domains on the active MHs in the NA, Murakami et al. [36] conducted a series of idealized seasonal predictions by modifying the predicted SSTs as lower boundary conditions. Using the same model and initial conditions, they reforecast the same 2017 summer except that the modified SSTs were prescribed in the lower boundary conditions (Fig. 12). Through a series of idealized experiments, replacing the Atlantic SSTs with the climatological mean SST (Fig. 12d) was found to exert a substantial impact on the predicted Atlantic MHs, although the La Niña-like SST anomaly in the Pacific did not play an important role (Fig. 12b). Specifically, modifying the SSTs over the MDR (Fig. 12f) changed the MHs significantly compared to the original experiment, indicating a key role played by the warm MDR SSTs on these active MHs in 2017. These results indicate that the SST anomaly over the tropical Atlantic was the most important cause of the active 2017 MH season in the NA. Murakami et al. [36] also conducted additional future experiments to mimic a similar summer to that in 2017 but in a future warmer climate. The 2017 SST anomalies (left-hand panel of Fig. 12a) were superimposed onto the future SSTs projected under the RCP4.5 and RCP8.5 experiments, separately. The greenhouse gas concentration in the model also modified to the anticipated future level. The numbers of projected MHs are shown in Fig. 13. Compared with the experiments prescribed with the 2017 SST anomalies superimposed on the mean present-day SSTs (CLIM+), the simulated numbers of MHs were larger for the experiments prescribed with the 2017 SST anomalies superimposed on the future mean SSTs (RCP4.5+ and RCP8.5+). These results indicate that increases in mean SST due to anthropogenic warming will amplify the risk of MHs in the future. Note that Murakami et al. [36] utilized predicted SSTs rather than observed SSTs for the lower boundary conditions in their idealized seasonal experiments, and this was because they started the attribution study during the 2017 hurricane season (i.e., real-time event attribution). One of the merits for real-time attribution studies using seasonal forecast models is that they can tell a forecaster about the relevant domains of SST anomalies, which is the most important aspect for hurricane activity even if the hurricane season is underway. Another advantage is to inform the public how much anthropogenic climate changes are

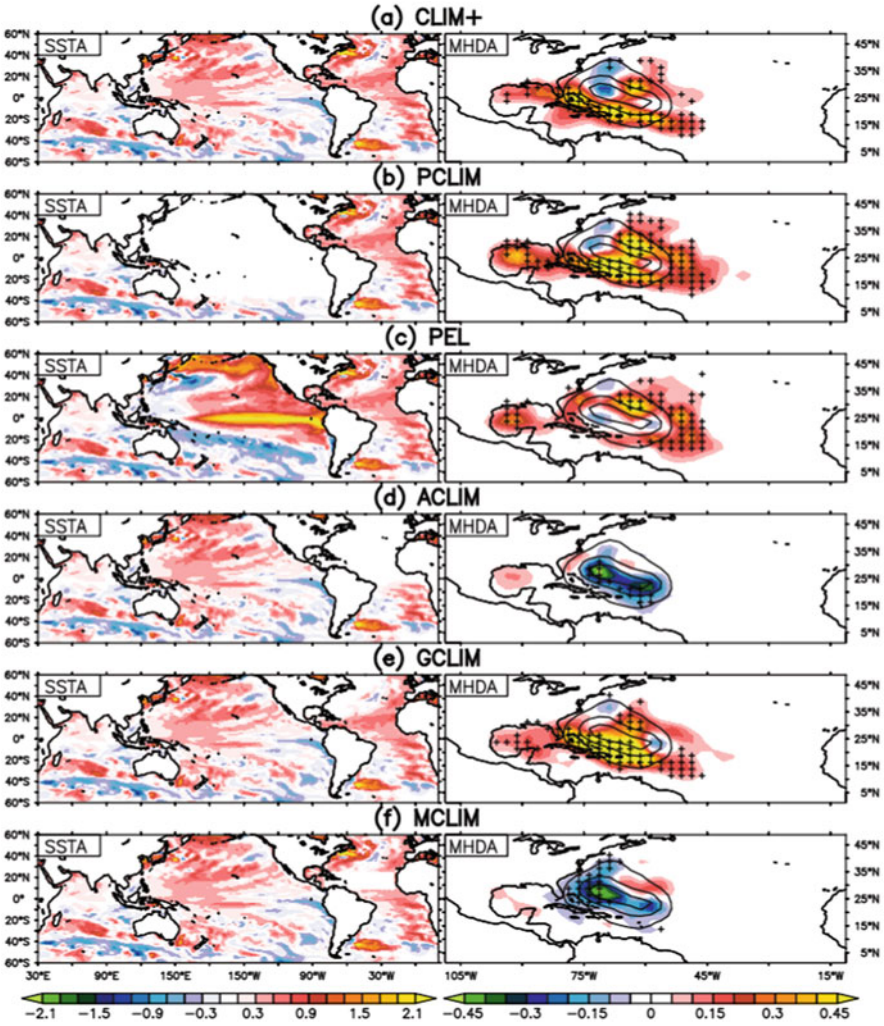

Fig. 12 Prescribed idealized sea surface temperature (SST) anomaly and resultant predicted major hurricane (MH) density by a seasonal prediction model. Idealized seasonal reforecasts conducted by prescribing the idealized SSTs in which SST anomalies (SSTAs; left-hand panels; units: K) are superimposed onto the climatological mean SST (CLIM). The resultant predicted MH density anomalies (MHDAs) relative to the CLIM experiment are shown by the shading in the right-hand panels (units: number per season). The prescribed SSTAs are (**a**) all 2017 anomalies (CLIM+); (**b**) as in CLIM+, except the Pacific SSTAs are set to zero (PCLIM); (**c**) as in CLIM+, except the Pacific SSTA is replaced with the SSTA predicted by 1 April 2017 initial predictions, predicting El Niño conditions (PEL); (**d**) as in CLIM+, except the Atlantic SSTA is set to zero (ACLIM); (**e**) as in CLIM+, except the SSTA off the coast of North America is set to zero (GCLIM); and (f) as in CLIM+, except the SSTA in the tropical Atlantic is set to zero. Contours in the right-hand panels denote the mean MH density predicted from the CLIM experiment. The contour interval is 0.6 per season. Cross marks in the right-hand panels indicate the predicted change relative to the CLIM experiment is statistically significant at the 90% confidence level or above. (Adapted from Murakami et al. [36]. @Science. Used with the author's copyright)

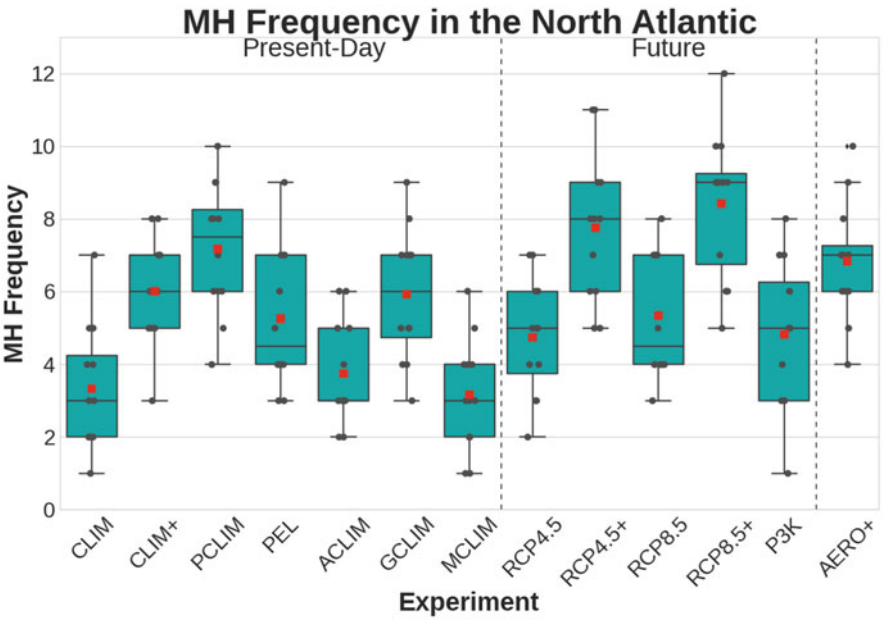

Fig. 13 Boxplots for the predicted major hurricane (MH) frequency over the North Atlantic according to various predicted sea surface temperature anomaly patterns. The red squares denote the ensemble mean, while the black dots show each ensemble member (12 members). The boxes represent the lower and upper quartiles; the horizontal lines in the middle show the median value; and the horizontal end lines show the lowest (highest) datum still within the 1.5 interquartile range of the lower (upper) quartile. (Adapted from Murakami et al. [36]. @Science. Used with the author's copyright)

relevant to the occurrence of an extreme hurricane season happening in real time. We can conduct these attribution experiments even after obtaining observed SSTs for more accurate estimation of the impact of SST anomalies on the active hurricane season. However, these observed SSTs are available only a few months behind real time, meaning timely information on the relationship between climate changes and extreme hurricane seasons is not available. A caveat is that event attribution using simulated SSTs assumes that the seasonal predictions of SSTs are accurate. Generally, due to the known spring predictability barrier phenomenon [38], tropical SST predictions initialized before spring show lower skill relative to those after spring. Therefore, long-lead-time seasonal predictions and attribution experiments initialized before spring could involve substantial uncertainty in their results; plus, there is also uncertainty related to the issue of model dependency, i.e., if a different model is used, the results could also be different.

A similar event attribution approach was also applied to the active TC season of 2018 in the Pacific [37]. There were 39 tropical storms (maximum surface wind speed $\geq$17.5 ms^{-1}) observed over the North Pacific in the 2018 TC season, with 8 storms becoming Category 5 super storms (maximum surface wind speed

$\geq$70.6 ms^{-1}) and 21 out of the 39 TCs making landfall. The observed number of storm days (SDAY; the total number of TC days throughout the TC's lifetime) was 228.3 for the 2018 TC season, exceeding 1.1 standard deviations above the mean. The 2018 TC season was characterized by moderate El Niño conditions, although the peak of the SST anomaly was in the tropical Central Pacific (Fig. 14a). There was also marked warming in the subtropical Pacific, practically associated with a positive phase of the Pacific Meridional Mode (PMM, Fig. 14a). The close connection between TCs in the Pacific and the PMM has been identified in previous studies [39]. Therefore, it is unclear which of the warm conditions—those generated by El Niño or PMM—caused the active TC season in 2018. Unlike Murakami et al. [36], Qian et al. [37] utilized three different dynamical models for their idealized attribution experiments, to avoid any dependency of the results on the model choice: (i) the Geophysical Fluid Dynamics Laboratory (GFDL) Forecast-oriented Low Ocean Resolution global coupled model (FLOR), (ii) the Meteorological Research Institute (MRI) Atmospheric General Circulation Model (MRI-AGCM3.2), and (iii) the Nonhydrostatic Icosahedral Atmospheric Model (NICAM). First, they showed that these three models reproduced the active 2018 TC season consistently in the Pacific via experiments in which SSTs were forced by predicted SSTs using a seasonal forecast model initialized on 1 July 2018 (Fig. 14a). Second, they conducted idealized experiments by modifying the SST anomaly; they replaced it with zero over the subtropical Pacific domain to estimate the effect of the warming induced by the PMM (Fig. 14b). The experiments with the modified SST resulted in a markedly decreased number of TCs over the Pacific, thus revealing a substantial impact of subtropical warming on the active TC season in 2018. Another experiment was forced with the same 2018 SST anomaly except that the tropical Pacific SST anomaly was replaced with zero (Fig. 14c). The experiments with the SST resulted in a similar SDAY to the original experiment (Figs. 14a, c), indicating that the moderate El Niño conditions were not responsible for the active TC season in the Pacific in 2018. Meanwhile, they also conducted future experiments like Murakami et al. [36] did, in which the 2018 SST anomaly was superimposed onto the mean SSTs in the future projected by FLOR under the RCP8.5 scenario along with the increased level of greenhouse gas. The projected SDAY showed inconsistent results across the different models (Fig. 14c). FLOR projected an increase in SDAY in the future, while MRI-AGCM3.2 projected a decrease. This inconsistency among the models highlights the considerable uncertainty in the projected future changes in SDAY in the Pacific. The model differences were specifically larger over the WNP than over other open oceans. Qian et al. [37] argued that the opposite sign of the projected change in SDAY over the WNP might come from the marked differences in the changes in atmospheric stability as defined by the difference in potential temperature between 200 hPa and 850 hPa, as well as strength of the Indo-Pacific Walker circulation. MRI-AGCM3.2 projected a large increase in atmospheric stability along with a large weakening of the Walker circulation, whereas FLOR projected a small increase in atmospheric stability and a small weakening of the Walker circulation. This uncertainty in the response of large-scale conditions to an increase in anthropogenic forcing leads to significant uncertainty in the projected future changes in TC activity.

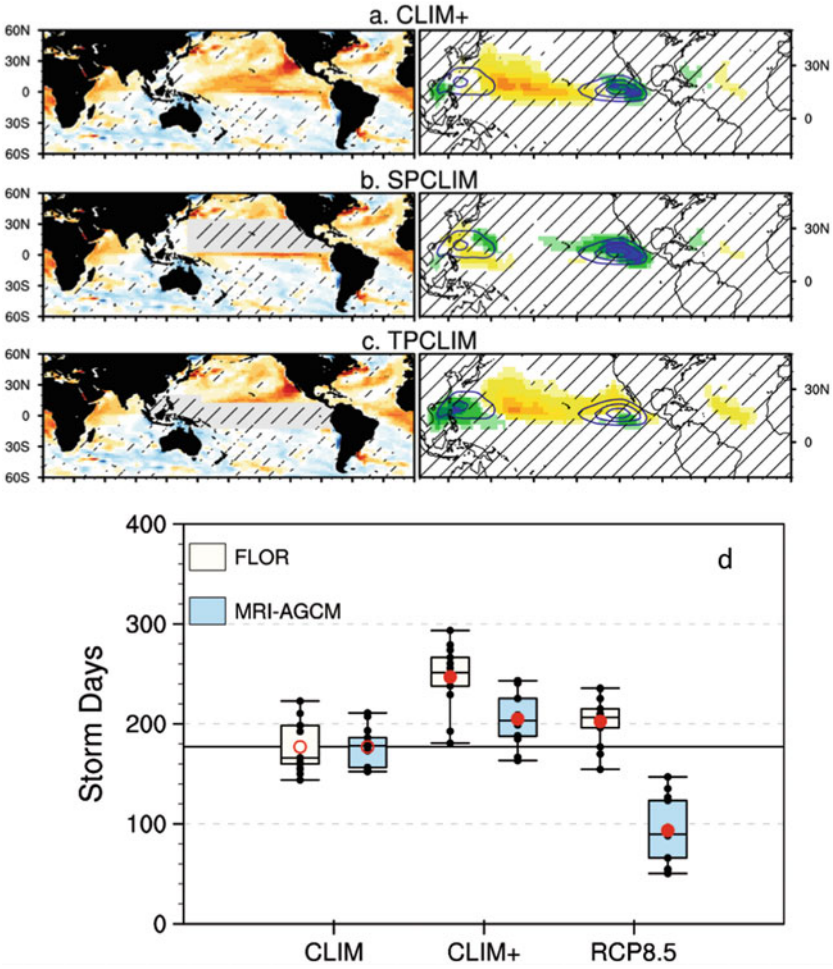

Fig. 14 Prescribed idealized sea surface temperature (SST) and storm day (SDAY) anomalies during the 2018 TC season. SDAY is defined as the total number of TC days throughout the lifetime of TCs counted for each 5° × 5° grid box for (**a**–**c**) and throughout the North Pacific for (**d**). Idealized seasonal prediction conducted by prescribing the idealized SSTs in which SST anomalies (shading in left-hand panels for **a**–**c**) are superimposed on the climatological mean SST. The resultant predicted multi-model ensemble mean of SDAY anomalies relative to the control experiments in which the climatological SSTs were prescribed is shown by the shading in (**a**–**c**). The contours in the right-hand panels in (**a**–**c**) indicate the climatological mean SDAY simulated by the control experiment. The prescribed SST anomalies are (**a**) all 2018 anomalies; (**b**) as in (**a**) except the SST anomalies in the subtropical Pacific are replaced with the climatological mean; and (**c**) as in (**a**) except the SST anomalies in the tropical Pacific are replaced with the climatological mean. Hatched areas in (**a**–**c**) indicate the changes relative to the control experiment on the grid cells are not statistically significant at the 95% confidence level. (**d**) Boxplots for the predicted basin total SDAY over the North Pacific. Red filled (hollow) dots indicate the simulated mean storm days simulated by the experiment is (not) statistically different from that of the control experiment (i.e., CLIM) at the 95% significance level. The horizontal line represents the ensemble mean of storm days in the control experiment. (Adapted from Qian et al. [37]. Used as open access)

Overall, unlike the Atlantic study by Murakami et al. [36], Qian et al. [37] concluded that it is unclear how much anthropogenic forcing impacted the occurrence of the active TC season in the North Pacific in 2018, due to model discrepancies. Their study highlights the importance of multi-model approaches to attribution studies owing to the uncertainty and model dependency on the effect of anthropogenic forcing to projected changes in large-scale conditions and TC activity.

7 Projected Increases in Global TC Numbers in the Future

Thus far, some recent studies related to observed or historical TC activity associated with anthropogenic climate changes have been reviewed. However, meanwhile, there have also been some new studies published on the projected future changes in TC activity, in which the results are somewhat different from past studies with a similar focus. This section reviews a few of the studies showing projected increases in global TC numbers in the future.

Many studies since the early 1990s have attempted to address the possible future changes in TC activity. Based on studies published since 2006, Knutson et al. [40] reviewed their findings and summarized the situation regarding the potential future changes in TC activity, as follows:

1. Theoretical and high-resolution model results project an increase in the mean maximum wind speed by 2–20% by the end of the twenty-first century.
2. Dynamical models project a decrease in the number of global TCs, by 6–34%, by the end of the twenty-first century under the Intergovernmental Panel on Climate Change (IPCC) A1B future scenario.

In addition, IPCC [1] discussed the potential future changes in TC activity by assessing previous studies using climate models. Because model projections often vary in terms of the details of the models, it is difficult to draw objective conclusions from their combined results to form a consensus. In IPCC [1], the model results were normalized using a combination of objective and subjective expert judgements. The results are summarized in Fig. 15. Potential future changes in TC activity were estimated for each ocean basin, as well as the hemispheric and global scale, in terms of the annual number of TCs (Metric I), the annual number of category 4–5 TCs (Metric II), the mean lifetime maximum TC intensity (Metric III), and the mean precipitation rate induced by TCs (Metric IV). Figure 15 reveals that Metric I is generally projected to decrease or remain unchanged in the next century globally as well as in most ocean basins, although confidence in the projections is lower in specific ocean basins than in global projections. Specifically, the models consistently projected a decreased number of TCs in the ocean basins in the Southern Hemisphere, while the projected future changes in the ocean basins of the Northern Hemisphere varied remarkably. In contrast, Metrics III and IV, which represent the mean TC intensity and TC precipitation rate, are relatively consistent among the model studies. These metrics generally show projected increases in most ocean

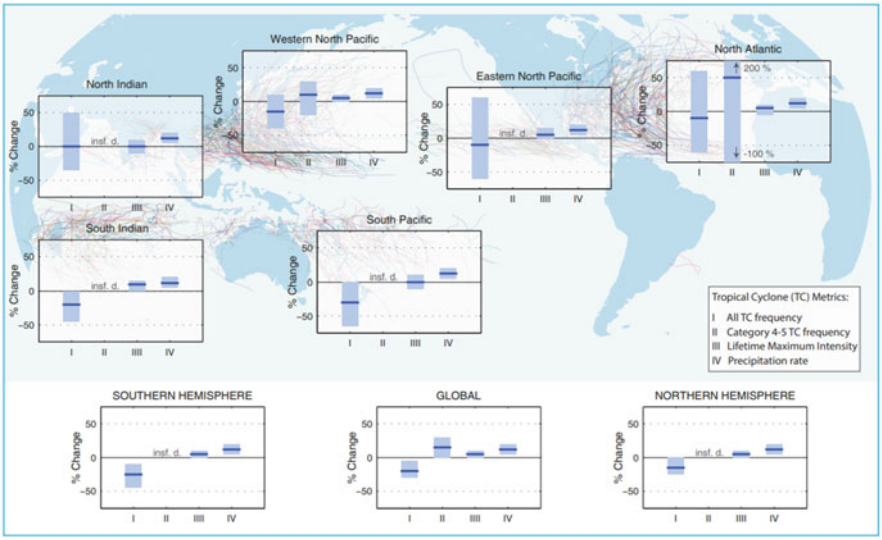

Fig. 15 Assessment of the projected future changes in tropical cyclone activity made by the Fifth IPCC report [1]. This consensus was reached by reviewing the modeling studies available by 2013. All values represent the expected percent change on average over the period 2081–2100 relative to 2000–2019, under an IPCC A1B-like scenario, based on expert judgement after subjective normalization of the model projections. Four metrics were considered: (*I*) the total annual number of tropical storms, (*II*) annual frequency of category 4 and 5 storms, (*III*) mean lifetime maximum intensity (LMI; the maximum intensity achieved during a storm's lifetime), and (*IV*) precipitation rate within 200 km of the storm center at the time of the LMI. For each plot, the solid blue line is the best guess of the expected percentage change, and the colored bar provides the 67% (likely) confidence interval for this value. (Adapted from IPCC [1])

basins as well as at the global scale. Based on these studies, IPCC [1] concluded that "It is *likely* that the global TC numbers will either decrease or remain essentially unchanged, concurrent with a *likely* increase in both global mean TC maximum wind speed and precipitation rates." Therefore, the science community to a certain extent agrees with the projected decrease in global TC numbers in the future based on the results of climate models, although the physical mechanism behind the decreases were still not clear.

However, there have been new studies published showing projected increases in the global number of TCs in the future. For example, Emanuel [41] applied a statistical–dynamical downscaling technique to the outputs of eight CMIP5 (phase 5 of the Coupled Model Intercomparison Project) climate models. In short, this downscaling technique applies a storm intensity model to TC tracks initiated by random seeding in space and time and forward-propagates using a beta and advection model driven by winds derived from the output of dynamical climate models. Note that in Emanuel [41], the rate of seed formation does not change with anthropogenic warming. The results showed a decreasing number of TCs globally

under the RCP4.5 scenario (medium emissions scenario) but an increasing number under the RCP8.5 scenario (high emissions scenario) relative to the present-day climate. Using the same downscaling technique except that the large-scale conditions were derived from the output of CMIP6 models, Emanuel [42] also projected an increasing number of global TCs in a warmer climate. Figure 16a shows the number of global TCs projected by the model. The blue line reveals the simulated TC number during the historical period (1850–2014), while the red line denotes the projected number of TCs under a future scenario in which the CO_2 level is increased by 1% per year from the present-day condition. This figure reveals significant projected increases in the global number of TCs under future anthropogenic warming. Emanuel [42] also showed that there is excellent correspondence between the simulated number of global TCs in his model and the Genesis Potential Index (GPI) calculated from the large-scale variables by CMIP6 models (green line in Fig. 16a). The GPI has been widely applied alongside climate models [e.g., 34] to diagnose the interannual and interdecadal variability of TC genesis towards better understanding the mechanisms responsible for the variability of TC genesis. Although there are several forms of GPI, the definition used in Emanuel [43] is as follows:

$$GPI = |\eta|^3 \chi^{\frac{4}{3}} MAX\left(\left(V_{pot} - 35\right), 0\right)^2 (25 + V_{shear})^{-4}, \tag{2}$$

where η is the absolute vorticity of the 850 hPa level, capped by 5×10^{-5} s^{-1}; V_{pot} is the potential intensity (hereafter referred to as PI); V_{shear} is the magnitude of the 850 hPa–250 hPa wind shear; and χ is the moist entropy deficit. The moist entropy deficit is defined as

$$\chi_m = \frac{s_m - s_m^*}{s_o^* - s_b}, \tag{3}$$

where s_m is the environmental moist entropy at 600 hPa, $s_m{}^*$ is the saturation entropy at 600 hPa in the inner core of a TC, $s_o{}^*$ is the moist entropy of air saturated at SST and pressure, and s_b is the moist entropy of the boundary layer. To calculate moist entropy, the pseudo-adiabatic entropy is defined as follows:

$$s = c_p \log(T) - R_d \log(p_d) + \frac{L_{vo} r_v}{T} - R_v r_v \log(H), \tag{4}$$

where c_p is the specific heat at constant pressure for dry air; T is the temperature; R_d is the gas constant for dry air; p_d is the partial pressure of dry air; L_{vo} is the latent heat of vaporization (set at 2.555×10^6J kg^{-1}); r_v is the water vapor mixing ratio; R_v is the gas constant for water vapor; and H is the relative humidity. PI represents an attainable maximum storm intensity that is theoretically derived given the three-dimensional thermodynamical large-scale conditions, such as atmospheric temperature, humidity, and SST. The formulation of PI is as follows:

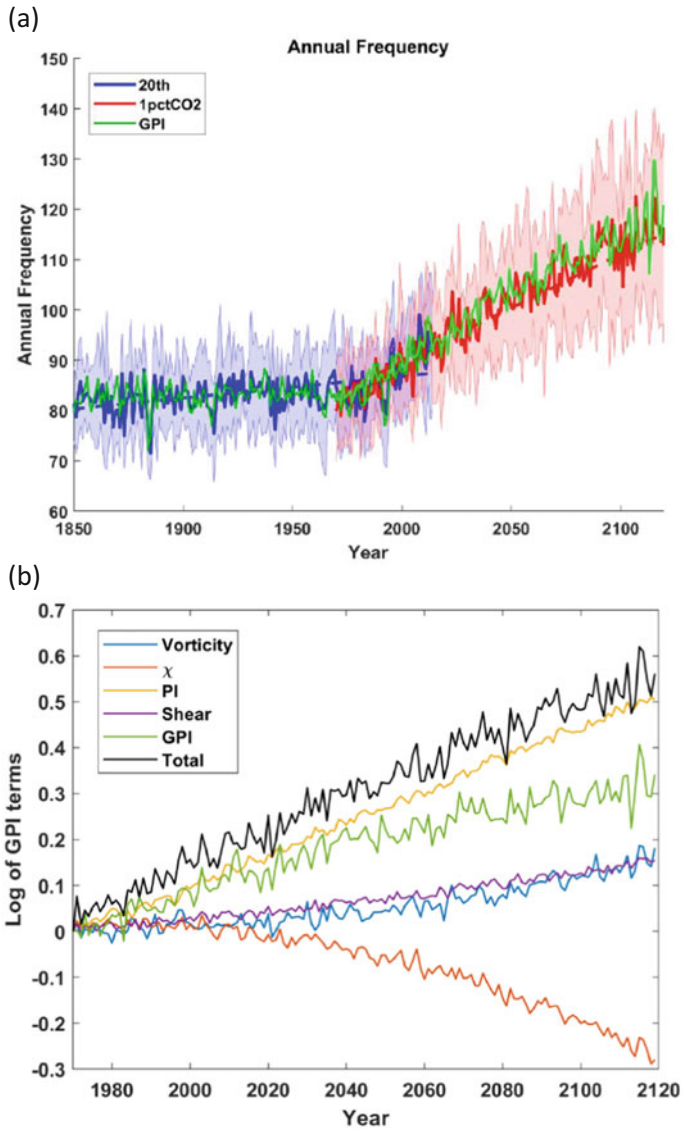

Fig. 16 (**a**) Annual global number of simulated tropical cyclones. Solid curves represent multi-model means, and shading indicates one standard deviation up and down. Dashed lines show linear regression trends. Blue indicates the historical period of 1850–2014, while red shows the 1% $yr.^{-1}$ CO_2 increase experiment beginning in 1970. Green curves show the multi-model mean, globally summed genesis potential index (GPI). (**b**) Each term's contribution to the total GPI in terms of the right-hand side of Eq. 6. The contributions are from vorticity, χ, potential intensity (PI), and vertical wind shear. The black curve shows their sum. (Adapted from Emanuel [42]. @American Meteorological Society. Used with permission)

$$u_{pi} \equiv \sqrt{\frac{C_k}{C_D}\frac{T_s - T_o}{T_o}\left(h_o^* - h^*\right)}, \tag{5}$$

where C_k is the surface enthalpy exchange coefficient; C_D is the surface momentum exchange coefficient; T_s is the SST; T_o is the outflow temperature; h_o^* is the saturation moist static energy of the sea surface; and h^* is the saturation moist static energy of the free troposphere. PI consists of two key factors: thermodynamic efficiency ($\frac{T_s - T_o}{T_o}$) and an air–sea disequilibrium term ($h_o^* - h^*$).

The GPI (Eq. 2) indicates that TC genesis is more favorable under a large-scale environment in which the background vorticity is cyclonic in the lower troposphere, the moist entropy deficit is larger, the PI is larger, and the vertical wind shear is smaller. This GPI was summed over the globe and averaged among the CMIP6 models that were used for the downscaling technique of Emanuel [40] (green line in Fig. 16a), and the results showed good agreement with the increase in the global number of TCs. The benefit of the GPI is that one can compute each term's contribution to the total GPI value. The logarithm is taken on both sides in Eq. 2, as follows:

$$\begin{aligned}\log\left(GPI\right) = {} & 3\log\left(\lfloor\eta\rfloor\right) - \frac{4}{3}\log\left(\chi\right) + 2\log\left(MAX\left(\left(V_{pot} - 35\right), 0\right)\right) \\ & - 4\log\left(25 + V_{shear}\right),\end{aligned} \tag{6}$$

Figure 16b shows the contribution of each term in Eq. 6 to the temporal evolution of the GPI, revealing that an increase in entropy deficit (red) could serve as a negative factor for the GPI. On the other hand, the negative effect from the entropy deficit is offset by a positive effect from the PI (yellow), as well as the vertical wind shear (magenta) and vorticity (blue). The PI becomes larger when the outflow temperature (i.e., temperature in the upper troposphere) becomes lower and/or the SST is higher. Given the projected increases in static stability in the future caused by the increased temperature in the upper troposphere, the projected increase in SST dominates the increased PI. It appears that the downscaling technique of Emanuel [42] is more sensitive to the thermodynamic parameters, especially the SST changes, although a number of dynamical climate models have shown a decreased global number of TCs despite the increase in SST under a warming climate. Despite the increased GPI associated with the PI, Emanuel [42] still did not articulate clear reasons for the projected increase in the global TC number by using the downscaling technique. Meanwhile, Emanuel [42] also indicted that the results of conventional dynamical models might have underestimated smaller-scale disturbances that became broader in structure in a warmer climate. It should be noted that most studies using conventional dynamical models explicitly simulated TCs with global atmospheric or coupled general circulation models whose horizontal resolutions varied from 14 to 200 km. Most of these models may under-resolve TCs, as well as the mesoscale process observed to be involved in their genesis. Simulated TCs that

develop in such models are detected using a storm-detection algorithm, and the counts of TCs are known to be sensitive to how that algorithm is formulated. Specifically, climate change may alter the scale of simulated TCs, pushing events across arbitrary detection thresholds and thereby leading to false trends in the number of weak events. For example, weaker TC-like disturbances could become broader as the climate warms, meaning their vorticity may decrease below the imposed vorticity thresholds used in many detection methods so that the detection algorithm may overlook TC genesis events with broader TC structure.

A similar statistical–dynamical downscaling technique was also developed and applied to CMIP5 models by Lee et al. [44]. Unlike the downscaling technique of Emanuel [42], in which the ratio of the number for the random seeding of TC genesis is fixed, Lee et al. [44] applied a variable seeding rate that depends on the environmental conditions through the GPI developed by Tippet et al. [45]. The seeding rate is formulated as follows:

$$\mu = \exp\left(b + b_\eta \eta_{850,c} + b_{CRH} CRH + b_{PI} PI + b_{SHR} SHR\right), \tag{7}$$

where μ is the estimated seeding rate; b is the intercept; b_X represents the coefficient of parameter X; η represents the absolute vorticity at 850 hPa, with the subscript c indicating that this GPI uses absolute vorticity clipped at 3.7×10^{-5} s^{-1}; CRH represents column-integrated relative humidity; PI represents potential intensity; and SHR represents deep-layer (850–250 hPa) vertical wind shear. This GPI is referred as CRH GPI. Tippet et al. [45] also proposed a slightly different GPI formulation as follows:

$$\mu = \exp\left(b + b_\eta \eta_{850,c} + b_{SD} SD + b_{PI} PI + b_{SHR} SHR\right), \tag{8}$$

where SD represents the saturation deficit, as defined in Eq. 3. Hereafter, this GPI is referred to as SD GPI. They computed monthly GPIs using the large-scale parameters derived from CMIP5 models running the historical and future experiments under the RCP8.5 scenario. Based on these GPIs, seeding rates were determined from Eq. 7 or 8, and a similar downscaling technique to that of Emanuel [42] was applied, in which advection model computes the trajectory of storms and a hurricane model simulates the storm intensity. Lee et al. [44] applied the downscaling by using the CRH GPI and SD GPI separately, and these experiments were referred to as TCGI_CRH and TCGI_SD, respectively. Figure 17 reveals that the projected future changes in the global number of TCs are totally the opposite between TCGI_CHR and TCGI_SD. When CRH was used, most of the results showed projected increases in TC numbers in the future, whereas, when SD was used, they showed projected decreases. The results were totally dependent on the random seeding rate (Fig. 17b), where SD GPI led to a decreasing trend toward the end of the twenty-first century, while CRH GPI led to an increasing trend in the random seeding rate. It is difficult to identify which of the results is the more plausible because both experiments showed similar evolution during the historical period (1980–2013) relative to observations (Fig. 17a). As indicated by Emanuel [42] and Lee et al. [44], the projected future

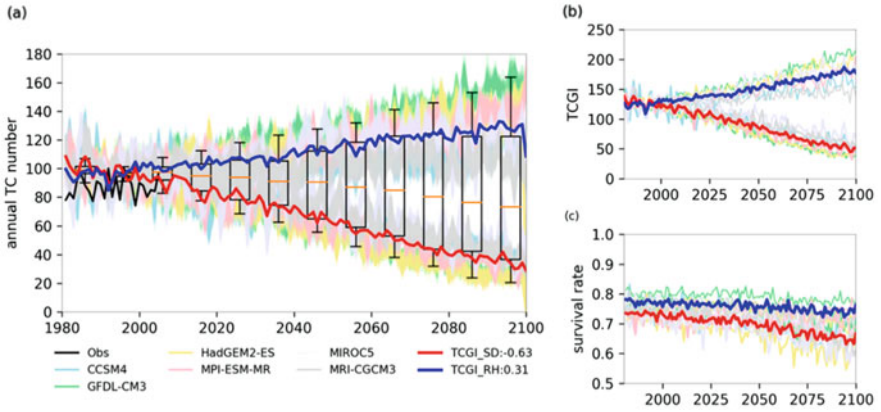

Fig. 17 Time series of (**a**) the simulated annual global number of tropical cyclones (TCs), (**b**) the simulated seeding rate, and (**c**) the survival rate of the synthetic storms. Thin lines show downscaling results from each of the CMIP5 models, indicated by color. The box-and-whisker diagram in (**a**) shows the median (orange) and the fifth, 25th, 75th, and 95th percentiles. The thick blue and red lines show the ensemble mean from the TCGI_CHR and TCGI_SD experiments, respectively. (Adapted from Lee et al. [44]. @American Meteorological Society. Used with permission)

changes in the global number of TCs are largely dependent on the large-scale parameters derived from global models. Specifically, the dependency of the results on the thermodynamic parameters is large in the statistical-downscaling technique. Previous studies indicate that the large-scale controlling variables for TC genesis would be different between the present-day climate and projected future climate [46, 47]. Specifically, the GPI formula had been optimized using reanalysis data to represent TC genesis frequency in the present-day climate. Because the validity of applying GPI formula to future climate had not been justified, the projected future changes in TC genesis number based on the GPI may include uncertainty in the statistical–dynamical technique.

There is also a dynamical climate model that projected an increase in the global number of TCs in a warmer climate. Vecchi et al. [48] utilized a coupled global climate model with increasingly refined atmosphere/land horizontal grids (50-km mesh GFDL FLOR model; 25-km mesh GFDL HiFLOR model). In a warmer climate forced with doubling CO_2 along with increased SST, the simulated global number of TCs markedly decreases in the FLOR model relative to the present-day climate, while the HiFLOR model shows an increasing change (blue bars in Fig. 18). They also conducted additional idealized experiments in which either CO_2 (gray bars in Fig. 18) or SST (red bars in Fig. 18) was increased separately. Both models showed an increasing number of TCs under increased SST only but a decreasing number of TCs under increased CO_2 only. However, HiFLOR showed larger (smaller) increases (decreases) under increased SST (CO_2) than FLOR did (Fig. 18). This indicates that the changes in the global number of TCs depend on the model's sensitivity to increasing CO_2 and SST. Vecchi et al. [48] also

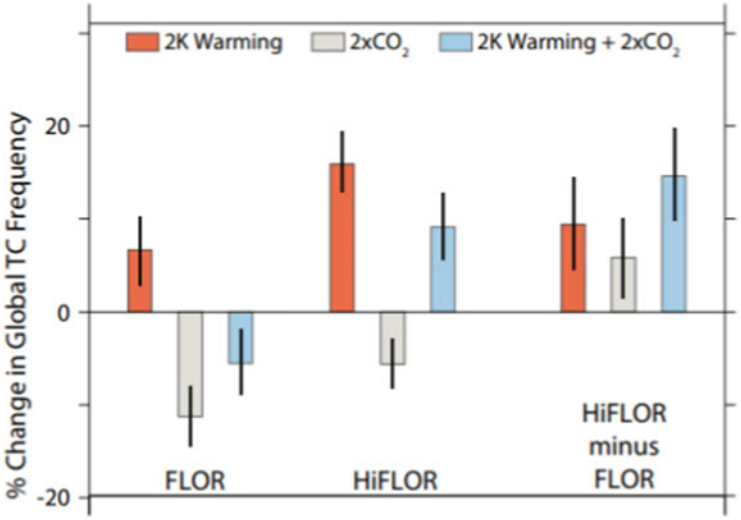

Fig. 18 Response of the global number of TCs in idealized experiments: leftmost bars are for the FLOR model; the second set of bars is for the HiFLOR model; and the rightmost bars show the difference between HiFLOR and FLOR. The blue bars show the response to a combined uniform 2 K warming and a CO_2 doubling, the gray bars show the response to CO_2 doubling with fixed SST, and the red bars show the response to a uniform 2 K warming. Black lines show the 95% confidence interval of the change. (Adapted from Vecchi et al. [48]. Used as open access)

investigated why HiFLOR projected an increasing global number of TCs in a warmer climate by analyzing projected changes in the large-scale parameters, such as the GPI developed by Emanuel [41] (Eq. 2), the ventilation index developed by Tang and Emanuel [49], and the vertical p-velocity with respect to the mass flux. These were all argued in past studies as potential causes for future changes in global TCs [42, 49–51]. The ventilation index was developed by Tang and Emanuel [49] and is a combination of entropy deficit and vertical wind shear, as follows:

$$\Lambda \equiv \frac{u_s \chi_m}{u_{pi}}, \tag{9}$$

where Λ is the non-dimensional ventilation index; u_s is vertical wind shear; χ_m is the entropy deficit, defined in Eq. 3; and u_{pi} is the potential intensity, defined in Eq. 5. A larger ventilation index implies an unfavorable large-scale environment for TC genesis and intensification.

First, the changes in the GPI (Fig. 19a) show positive correlations with the model-simulated changes in the global number of TCs within the individual models of FLOR and/or HiFLOR (red and gray lines). However, it cannot explain the differences between models. For example, even with the same degree of changes in the GPI, HiFLOR tends to project increased storm numbers, while FLOR tends to project decreased storm numbers. Second, the changes in ventilation index (Fig. 19b) do not account for both the intra- and inter-model differences in the

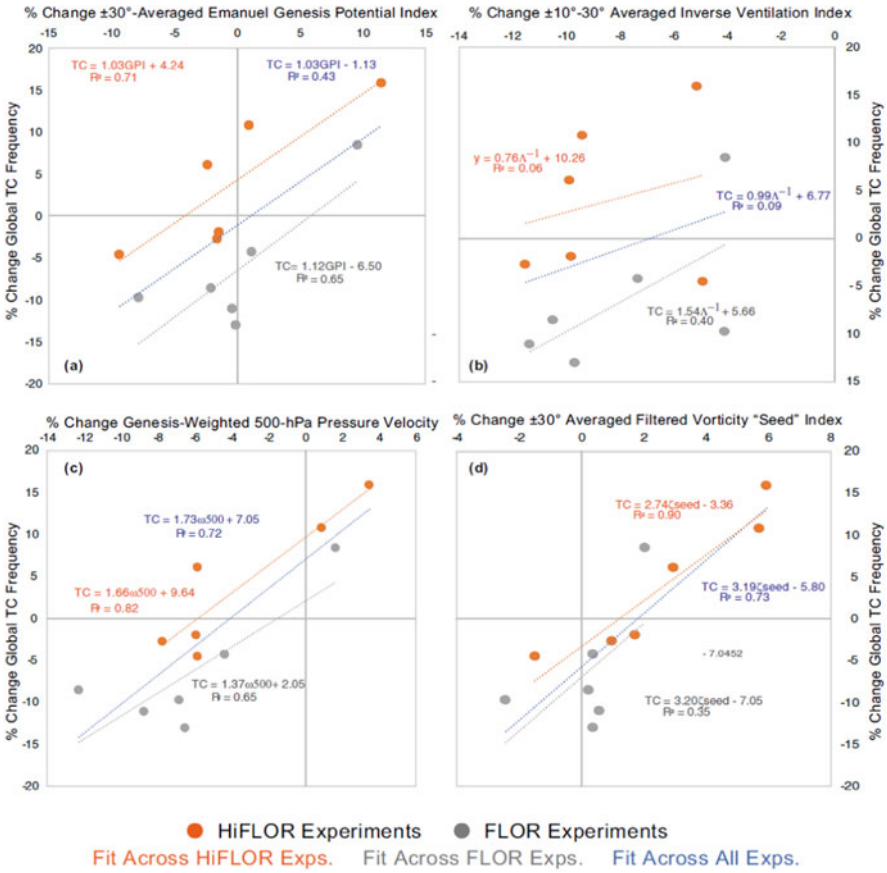

Fig. 19 Fractional response in the global number of tropical cyclones (TCs) versus the fractional response in spatially averaged large-scale parameters. Orange symbols show the responses of the HiFLOR model and gray symbols those of the FLOR model. The dotted lines indicate the linear least-squares regression fit with the covariance indicated by R^2. Orange lines show the regression for HiFLOR points, gray for FLOR points, and blue for all data combined. Each symbol is the response of one idealized experiment relative to the present-day control experiment (e.g., doubling CO_2 experiments, +2 K uniform SST experiments, and the combined experiments). Fractional response of the simulated global TC number is compared with the (**a**) tropical-mean response of the GPI of Emanuel [41] (Eq. 8), (**b**) ± 10–30° averaged inverse Tang and Emanuel ventilation index [49], (**c**) 500 hPa pressure velocity, and (**d**) tropical cyclones "seed" index [53]. (Adapted from Vecchi et al. [48]. Used as open access)

changes in storm number. Third, it appears that the changes in vertical *p*-velocity (Fig. 19c) are highly correlated with those in storm number relative to the GPI and ventilation index. However, the regression lines show different offsets between FLOR and HiFLOR, revealing different sensitivities of *p*-velocity to storm number in these models. In summary, none of the large-scale parameters perfectly reflects both the intra- and inter-model differences in the changes in storm number. Vecchi

et al. [48] further hypothesized that the projected changes in TC number are influenced by the rate of pre-storm synoptic-scale disturbances: so-called TC seeds. Because TCs originate from tropical disturbances such as synoptic wave trains and easterly waves [e.g., 52], the number of TCs could depend on the likelihood that these seeds develop into TCs. Moreover, the projected changes in the number of TC seeds could be independent of those in the large-scale parameters. Following Li et al. [53], Vecchi et al. [48] analyzed a "seed index" in which the variance of 3–10-day relative vorticity fields at 850 hPa was computed after removing the TCs from the original vorticity fields. Figure 19d reveals that the seed index represents both the intra- and inter-model differences among the model experiments. Moreover, the regression lines are similar for the two models, indicating its potential to be a universal index that quantifies the projected changes in the global number of TCs in any climate model. Vecchi et al. [48] also noted that TC genesis is a binomial process, in which the expected number of TCs depends on the product of the number of seeds (i.e., trials) and the probability of success of each trial developing into TC genesis. The large-scale parameter could influence the latter. This hypothesis indicates that, even when the probability of a seed developing into TC genesis is small as determined by the negative large-scale conditions, the number of TC geneses could increase in cases with a larger number of seeds. Indeed, HiFLOR projected an increase in seeds in a warmer climate, which was the main reason for the projected increases in TC numbers despite the unfavorable large-scale conditions, such as an increase in the mean ventilation index and decrease in the mean upward p-velocity. Furthermore, Hsieh et al. [54] separated the development of a TC into three stages, from a non-rotating convective cluster to a weakly rotating seed and to a strongly rotating TC. They revealed that the initiation of convective clusters follows the large-scale vertical velocity, the transition to seeds is controlled by the large-scale vorticity, and the transition to TCs is controlled by entropy ventilation so that different large-scale parameters differently and complicatedly control TC genesis. Although HiFLOR showed an increase in the number of TC seeds in a warmer climate, it remains unclear as to what controls the number of seeds. Sugi et al. [55] reported that two different dynamical models showed projected decreases in the number of TC seeds in a warmer climate. Further studies are needed in the future to clarify the projected changes in TC seeds and the physical mechanisms dictating future changes in TCs.

8 Conclusion

This chapter has reviewed the observed climate changes in TCs over the last few decades, as well as the projected future changes through the latest numerical modeling studies that had not been covered in the previous literature reviews [13, 14]. Generally, it is challenging to detect any long-term climatic changes in global TC activity from observations because the availability of a reliable historical record of TCs is limited before satellite observations began to be made around the 1980s. Also, there are substantial effects from natural multidecadal variability

on global TC activity. Although some trends in the short-term observed record appear to be statistically significant, it is difficult to distinguish such trends from intrinsic multidecadal internal variability. However, given the now 40-year accumulation of a reliable observed global TC record, in addition to recent advancements made in the field of numerical climate modeling, some of the latest studies have shed light on the effect of ongoing anthropogenic climate changes on the trends in observed TCs. On the other hand, several recent modeling studies have revealed substantial uncertainty regarding the potential future changes in global TC activity.

Murakami et al. [18] revealed that climate changes in global TC activity during 1980–2018 were more evident in terms of the spatial pattern of TC occurrence, rather than the overall global number of TCs. There is a distinct spatial pattern of the trends in TCF (or TC density) on a global scale since 1980, with substantial reductions in the South Indian Ocean and WNP and increases in the NA and Central Pacific. They applied a new "large-ensemble simulation" technique with fully coupled global climate models that allows one to better define a model's forced response and distinguish it from modeled natural variability, taking advantage of ensemble statistics given a sufficiently large ensemble. They found that external forcing, such as greenhouse gases, anthropogenic aerosols, and volcanic eruptions, likely played an important role in the observed trend in TCF over the period 1980–2018. They also indicated that the two volcanic eruptions that occurred in the Northern Hemisphere in the 1980s and 1990s likely exerted substantial influence on the global TCF by altering the hemispheric meridional gradient of surface temperature, which in turn led to a meridional shift in TCF, as also indicated by another recent study [20]. On the other hand, the model experiments forced only with increased CO_2, while other external forcings were kept unchanged showing decreasing trends in TCF over the NA, which was opposite to the experiments forced with all external forcings. These mixed results suggest that the observed positive trends in TCF in the NA over 1980–2018 could be partially attributable to the diminishing effect of anthropogenic aerosols, which is in line with the literature [23, 24]. Overall, the climate models used by Murakami et al. [18] projected decreasing trends in the number of TCs in the NA toward the end of the twenty-first century because of the dominant effect of increased CO_2. Their study highlighted the mixed effect of anthropogenic forcing on TC activity: CO_2 increases may lead to decreases in TCs over the NA, while decreasing anthropogenic aerosols may lead to increases. Additional large-ensemble experiments that are forced with a single external forcing will be useful to clarify the impact of individual forcings on the global activity of TCs.

There are a few new studies that have reported significant observed trends in TC activity near the world's coastlines since the 1980s. For example, Wang and Toumi [26] reported that the distance between the point of TC maximum intensity and the nearest land mass has decreased by about 30 km per decade and that the annual frequency of global TCs has increased with proximity to land by about two additional cyclones per decade since 1982. Consistent with this, the fraction of annual TCs entering coastal regions and the annual mean fraction of their lifetime that TCs spend in coastal regions

have increased with proximity to land. These observed trends suggest a global-scale landward migration of TC activity, leading to substantial increases in TC risk. Wang and Toumi [26] also found that the observed increases in the annual mean fraction of their lifetime that TCs spend in coastal regions were not relevant to the slowdown in the mean moving velocity of TCs, but were related to the increases in TC genesis and TCF near the world's coastal regions associated with changes in the large-scale atmosphere and ocean conditions. Wang and Toumi [26] also considered a possible influence by multidecadal natural variability (e.g., the PDO), but they found that the observed increases were still present even when only PDO-neutral years were considered for the trend analysis. Another study related to that of Wang and Toumi [26] found that TCs approaching Tokyo have been increasing in frequency since 1980 [27]. However, because these studies were based on observational analysis only, no clear evidence has been shown as to whether these trends have been caused by anthropogenic climate changes.

Other observational studies have reported a slower decay of landfalling TCs in land regions adjacent to the NA [28] and WNP [30]. Given that many climate modeling studies project increases in mean TC intensity in a warmer climate, it was hypothesized that the mean duration of a TC over land could be longer because of the increased TC intensity at the time of landfall, meaning it takes longer for dissipation over land to occur. However, Li and Chakraborty [28] reported through idealized numerical experiments that, even under the same TC intensity at landfall, TCs can last longer over land when the local SST is higher. This result rejects the above hypothesis and indicates that it is not the initial TC intensity at landfall but the total amount of moisture in the air that determines the duration of a TC over land. Liu et al. [30] also showed an increasing trend in the annual mean overland duration of a TC over mainland China during the period 1975–2009. Consistent with the conclusion of Li and Chakraborty [28], they showed that observed decreases in the intensity weakening rate after landfall were responsible for the longer duration of TCs over land, which might be linked to the increasing SSTs in the coastal region of mainland China.

The increasing frequency of extremely severe TCs in some regions and unprecedented extreme hurricane season events in recent decades have aroused public interest regarding the effect of global warming on the occurrence of these events. Because most previous studies examined projected future changes in mean TC activity over a specific period, such as a few decades at the end of this century, these studies were limited to identifying if individual events of storms or seasons have been driven by anthropogenic climate changes. To address the gap between public and scientific interests, a new "event attribution" technique has been applied to individual events of storms and seasons.

One such technique, which involves the so-called pseudo-global warming experiments, was applied to individual storms to quantify the effect of climate changes on the increasing TC intensity in terms of maximum wind speed and precipitation. This technique resembles medium-range weather forecasting, except that the background thermodynamic variables, such as air temperature and

humidity, are forced as lateral boundary conditions. The same forecast simulations are conducted but forced with modified large-scale variables in which the effect of global warming is removed or superimposed. The counterfactual simulations are compared with the original simulations to see how much the changing mean state caused by global warming could alter TC statistics such as TC intensity. Patricola and Wehner [32] applied pseudo-global warming experiments to 15 major TC events over the NA and Pacific oceans. They concluded that future anthropogenic warming would robustly increase the TC maximum wind speed and rainfall of 11 of 13 intense TCs. In contrast, they showed that the climate change between the present-day and pre-industrial conditions so far might have enhanced the average and extreme rainfall for several hurricanes but might not have changed the TC maximum wind speed. Similar pseudo-global warming experiments were conducted by Reed et al. [33] for Hurricane Florence, and the results showed that the simulated total accumulated rainfall over land induced by Hurricane Florence increased significantly when compared with the counterfactual experiments that mimicked the pre-industrial climate. They also reported that Hurricane Florence would be about 80 km larger in size because of climate change. Although these studies are useful to estimate the effect of climate change on TC intensity for individual storms, there is a caveat to this technique; that is, it assumes that the simulated TC track will not change in a different mean climate state. Indeed, several studies have already reported that global warming will also alter the tracks of TCs. Moreover, a pseudo-warming experiment cannot quantify how much a changing climate will alter the frequency of occurrence of extreme storms, because these experiments are conducted using the initial conditions in which the target TCs were already included. Another issue with this event attribution studies is that they are completely dependent on models for the attribution, and they also typically do not demonstrate that there has been a detectable change in a relevant observed time series to support the inferences from the model.

Another event attribution study was applied to seasonal predictions. Murakami et al. [36] utilized a seasonal prediction model to identify the cause of the active MH season in the NA in 2017. They first showed that their dynamical seasonal prediction model could predict the active MH season in 2017 a few months in advance. Then, they applied idealized seasonal forecast experiments in which the same seasonal predictions were performed using the dynamical model but forced with the SST simulated by the seasonal predictions with some modifications to identify which region of SST anomalies were responsible for the active MH season. Murakami et al. [36] found that the warm SSTs over the tropical NA were the primary reason for the active MH season in 2017, while the moderate La Niña conditions that same year were a minor influence. They also conducted idealized seasonal predictions for the future conditions in which the projected future increases in the mean SSTs were superimposed onto the 2018 SST fields to mimic the 2018 summer conditions but under the anticipated future climate at the end of this century by prescribing anticipated future level of CO_2. They found that a more active MH season than that in 2018 was projected using the future SSTs,

indicating a substantial influence of global warming on the occurrence of an active MH season like that in 2018. A similar event attribution study was applied to the 2019 active TC season over the WNP by Qian et al. [37]. Different from the approach of Murakami et al. [36], they utilized three different dynamical models to test the sensitivity of the results to the choice of model. Although they found that warmer SSTs over the central Pacific were the primary reason for the active TC season in 2018 and that the results were consistent among the three models, the future experiments showed diverse results. Their study highlights the importance of a multi-model approach to quantifying the uncertainty in future projections.

There have also been some recent studies showing different projected future increases in the global number of TCs to previous studies. By applying a statistical–dynamical technique, Emanuel [42] reported projected future increases in the global number of TCs in a warmer climate, and they also reported that this projected increase was highly correlated with the GPI computed from the large-scale variables that forced the statistical–dynamical downscaling. Specifically, they showed that the projected increases in TC number may be related to the thermodynamic parameters, such as the PI. On the other hand, Lee et al. [44] also conducted future projections using different statistical–dynamical models in which the TC genesis rate depended on the GPI. They showed that this downscaling using the GPI based on relative humidity resulted in a projected increase in the global number of TCs, whereas using the GPI based on saturation deficit resulted in a projected decrease. These contradictory results highlight the substantial level of uncertainty in the projected future changes of TC genesis. Another recent study used a high-resolution dynamical global model to show a projected increase in the global number of TCs in a warmer climate [48]. Specifically, they revealed that the projected future changes in TC genesis depended on two factors: the TC seeding rate and the probability of a seed developing into a TC. They showed that the projected future changes in large-scale mean variables primarily modified the latter. However, even if the large-scale mean variables were unfavorable for TC development, the number of TCs could be increased in cases with increased TC seeds. Indeed, the climate model used in Vecchi et al. [48] showed projected future increases in TC seeds even when the large-scale conditions such as the ventilation index and mean vertical motion became more unfavorable for TC development. However, another recent study by Sugi et al. [50] indicated that different dynamical models projected decreased numbers of TC seeds in a warmer climate. Overall, projected future changes in the global number of TCs remain highly uncertain. Moreover, there is no established theory as to how the global number of TCs is determined. More theoretical and experimental studies are needed to clarify the future changes in TC genesis.

Finally, Fig. 20 summarizes the updated consensus among the science community regarding the possible projected future changes in TC activity [14]. The consensus has not changed relative to IPCC [1], as shown in Fig. 15. However, one major difference from Fig. 15 can be recognized at the global scale, whereby a larger

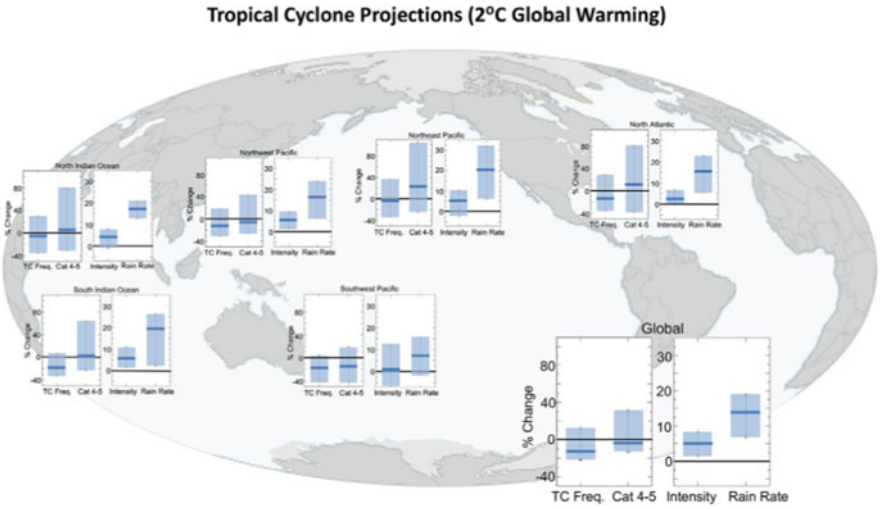

Fig. 20 Summary of tropical cyclone (TC) projections for a 2 °C global anthropogenic warming reported in Knutson et al. [14]. Like Fig. 15, shown for each basin and the globe are the median and percentile ranges for projected percentage changes in TC frequency, category 4–5 TC frequency, mean TC intensity, and TC rain rates. For storm frequency, the 5th–95th-percentile range across published estimates is shown. For category 4–5 storm frequency, mean TC intensity, and TC rain rates, the 10th–90th-percentile range is shown. (Adapted from Knutson et al. [14]. © American Meteorological Society. Used with permission)

uncertainty range in the global number of TCs is apparent. This increased uncertainty is mainly because experts have considered the abovementioned new studies in which projected increases in the global number of TCs have been shown. Knutson et al. [14] concluded lower confidence regarding a decrease in the global TC number. Instead, they showed medium-to-high confidence in an increase in the proportion of TCs that reach very intense levels.

In conclusion, future projections as well as ongoing climate changes in TC activity remain a challenging scientific topic despite considerable progress having been made in response to the sizeable societal impacts involved and therefore the substantial level of public interest. There are large uncertainties in the future projections of TC numbers, as well as the regional changes in TC activity. Reducing these uncertainties in climate model projections is important. Understanding the physical mechanisms controlling TC genesis is also an important topic. It is expected that accumulating reliable observations of TCs over the long term will help towards a better understanding of the effect of climate change on TC activity. New studies using climate models, long-term observations, and theories are needed to shed further light on the uncertainties involved in projecting the future patterns and trends of TCs.

Acknowledgments The authors thank Dr. Tom Knutson and Dr. Pang-Chi Hsu for their suggestions and comments.

References

1. IPCC (2013) Climate change 2013: the physical science basis. Cambridge University Press, Cambridge., 1535 pp. https://doi.org/10.1017/CBO9781107415324
2. Velden C et al (2006) The Dvorak tropical cyclone intensity estimation technique: a satellite-based method that has endured for over 30 years. Bull Am Meteor Soc 87:1195–1210. https://doi.org/10.1175/BAMS-87-9-1195
3. Kossin JP, Olander TL, Knapp KR (2013) Trend analysis with a new global record of tropical cyclone intensity. J Clim 26:9960–9976. https://doi.org/10.1175/JCLI-D-13-00262.1
4. Mantua NJ, Hare SR, Zhang Y, Wallace JM, Francis RC (1997) A Pacific interdecadal climate oscillation with impacts on salmon production. Bull Am Meteor Soc 78:1069–1079. https://doi.org/10.1175/1520-0477(1997)078<1069:APICOW>2.0.CO;2
5. Folland CK, Parker DE, Colman A, Washington R (1999) Large scale modes of ocean surface temperature since the late nineteenth century. In: Navarra A (ed) Beyond El Niño: Decadal and Interdecadal Climate Variability. Springer-Verlag, Berlin, pp 73–102
6. Delworth TL, Mann ME (2000) Observed and simulated multidecadal variability in the Northern hemisphere. Clim Dyn 16:661–676. https://doi.org/10.1007/s003820000075
7. Li W, Li L, Deng Y (2015) Impact of the interdecadal Pacific oscillation on tropical cyclone activity in the North Atlantic and Eastern North Pacific. Sci Rep 5:12358. https://doi.org/10.1038/srep12358
8. Zhao J (2018) Contribution of the interdecadal Pacific oscillation to the recent abrupt decrease in tropical cyclone genesis frequency over the western North Pacific since 1998. J Clim 31:8211–8224. https://doi.org/10.1175/JCLI-D-18-0202.1
9. Yan X, Zhang R, Knutson TR (2017) The role of Atlantic overturning circulation in the recent decline of Atlantic major hurricane frequency. Nat Commun 8:1695. https://doi.org/10.1038/s41467-017-01377-8
10. Klotzbach PJ, Gray WM (2008) Multidecadal variability in North Atlantic tropical cyclone activity. J Clim 21:3929–3935. https://doi.org/10.1175/2008JCLI2162.1
11. Pielke RA, Landsea C, Mayfield M, Laver J, Pasch R (2005) Hurricanes and global warming. Bull Am Meteor Soc 86:1571–1575. https://doi.org/10.1175/BAMS-86-11-1571
12. Bell GD, Chelliah M (2006) Leading tropical modes associated with interannual and multi-decadal fluctuations in North Atlantic hurricane activity. J Clim 19:590–612. https://doi.org/10.1175/JCLI3659.1
13. Knutson T et al (2019) Tropical cyclones and climate change assessment: part I. Detection and attribution. Bull Am Meteor Soc 100:1987–2007. https://doi.org/10.1175/BAMS-D-18-0189.1
14. Knutson T et al (2020) Tropical cyclones and climate change assessment: part II. Projected response to anthropogenic warming. Bull Am Meteor Soc 101:E303–E322. https://doi.org/10.1175/BAMS-D-18-0194.1
15. Wang C, Wu K, Wu L, Zhao H, Cao J (2021) What caused the unprecedented absence of Western North Pacific tropical cyclones in July 2020? Geophys Res Lett 48:e2020GL092282. https://doi.org/10.1029/2020GL092282
16. Murakami H, Vecchi GA, Delworth TL, Wittenberg AT, Underwood S, Gudgel R, Yang X, Jia L, Zeng F, Paffendorf K, Zhang W (2017) Dominant role of subtropical Pacific warming in extreme eastern Pacific hurricane seasons: 2015 and the future. J Clim 30:243–264. https://doi.org/10.1175/JCLI-D-16-0424.1
17. Murakami H, Vecchi GA, Underwood S (2017) Increasing frequency of extremely severe cyclonic storms over the Arabian Sea. Nat Clim Chang 7:885–889. https://doi.org/10.1038/s41558-017-0008-6
18. Murakami H, Delworth TL, Cooke WF, Zhao M, Xiang B, Hsu PC (2020) Detected climatic change in global distribution of tropical cyclones. Proc Natl Acad Sci U S A 117(20):10706–10714. https://doi.org/10.1073/pnas.1922500117

19. Lehner F, Deser C, Maher M, Marotzke J, Fischer E, Brunner L, Knutti R, Hawkins D (2020) Partitioning climate projection uncertainty with multiple large ensembles and CMIP5/6. Earth Syst Dynam. https://doi.org/10.5194/esd-2019-93
20. Pausata FSR, Camargo SJ (2019) Tropical cyclone activity affected by volcanically induced ITCZ shift. Proc Natl Acad Sci U S A 116(16):7732–7737. https://doi.org/10.1073/pnas.1900777116
21. Evan AT (2012) Atlantic hurricane activity following two major volcanic eruptions. J Geophys Res 117:D06101. https://doi.org/10.1029/2011JD016716
22. Camargo SJ, Polvani LM (2019) Little evidence of reduced global tropical cyclone activity following recent volcanic eruptions. Npj Clim Atmos Sci 2:14. https://doi.org/10.1038/s41612-019-0070-z
23. Dunstone NJ, Smith DM, Booth BBB, Hermanson L, Eade R (2013) Anthropogenic aerosol forcing of Atlantic tropical storms. Nat Geosci 6:534–539. https://doi.org/10.1038/ngeo1854
24. Sobel AH, Camargo SJ, Hall TM, Lee CY, Tippett MK, Wing AA (2016) Human influence on tropical cyclone intensity. Science 353:242–246. https://doi.org/10.1126/science.aaf6574
25. Kossin JP, Emanuel KA, Vecchi GA (2014) The poleward migration of the location of tropical cyclone maximum intensity. Nature 509:349–352. https://doi.org/10.1038/nature13278
26. Wang S, Toumi R (2021) Recent migration of tropical cyclones toward coasts. Science 372: 514–517. https://doi.org/10.1126/science.abb9038
27. Yamaguchi M, Maeda S (2020) Increase in the number of tropical cyclones approaching Tokyo since 1980. J Meteor Soc Jpn 98:775–786. https://doi.org/10.2151/jmsj.2020-039
28. Li L, Chakraborty P (2020) Slower decay of landfalling hurricanes in a warming world. Nature 587:230–234. https://doi.org/10.1038/s41586-020-2867-7
29. Chen X, Wu L, Zhang J (2011) Increasing duration of tropical cyclones over China. Geophys Res Lett 38:L02708. https://doi.org/10.1029/2010GL046137
30. Liu L, Wang Y, Zhan R, Xu J, Duan Y (2020) Increasing destructive potential of landfalling tropical cyclones over China. J Clim 33:3731–3743. https://doi.org/10.1175/JCLI-D-19-0451.1
31. Wehner MF, Zarzycki C, Patricola C (2019) Estimating the human influence on tropical cyclone intensity as the climate changes. In: Collins J, Walsh K (eds) Hurricane risk, vol 1. Springer, Cham
32. Patricola CM, Wehner MF (2019) Anthropogenic influenced on major tropical cyclone events. Nature 563:339–346. https://doi.org/10.1038/s41586-018-0673-2
33. Reed KA, Stansfield AM, Wehner MF, Zarzycki CM (2020) Forecasted attribution of the human influence on hurricane Florence. Sci Adv 6:eaaw9253. https://doi.org/10.1126/sciadv.aaw9253
34. Murakami H, Wang B (2010) Future change of North Atlantic tropical cyclone tracks: projection by a 20-km-mesh global atmospheric model. J Clim 23:2699–2721. https://doi.org/10.1175/2010JCLI3338.1
35. Colbert AJ, Soden BJ, Vecchi GA, Kirtman BP (2013) The impact of anthropogenic climate change on North Atlantic tropical cyclone tracks. J Clim 26:4088–4095. https://doi.org/10.1175/JCLI-D-12-00342.1
36. Murakami H, Levin E, Delworth TL, Gudgel R, Hsu PC (2018) Dominant effect of relative tropical Atlantic warming on major hurricane occurrence. Science 362:794–799. https://doi.org/10.1126/science.aat6711
37. Qian Y, Murakami H, Nakano M, Hsu PC, Delworth TL, Kapnick SB, Ramaswamy V, Mochizuki T, Morioka Y, Doi T, Kataoka T, Nasuno T, Yoshida K (2019) On the mechanisms of the active 2018 tropical cyclone season in the North Pacific. Geophys Res Lett 46: 12293–12302. https://doi.org/10.1029/2019GL084566
38. Duan W, Wei C (2013) The spring predictability barrier for ENSO predictions and its possible mechanism: results from a fully coupled model. Int J Climatol 33(5):1280–1292. https://doi.org/10.1002/joc.3513
39. Zhang W, Vecchi GA, Murakami H, Villarini G, Jia L (2016) The Pacific meridional mode and the occurrence of tropical cyclones in the western North Pacific. J Clim 29:381–398. https://doi.org/10.1175/JCLI-D-15-0282.1

40. Knutson TR et al (2010) Tropical cyclones and climate change. Nat Geosci 3:157–163. https://doi.org/10.1038/ngeo779
41. Emanuel K (2013) Downscaling CMIP5 climate models shows increased tropical cyclone activity over the 21st century. Proc Natl Acad Sci U S A 110:12219–12224. https://doi.org/10.1073/pnas.1301293110
42. Emanuel K (2021) Response of global tropical cyclone activity to increasing CO_2: results from downscaling CMIP6 models. J Clim 34:57–70. https://doi.org/10.1175/JCLI-D-20-0367.1
43. Emanuel K (2010) Tropical cyclone activity downscaled from NOAA-CIRES reanalysis, 1908–1958. J Adv Model Earth Sys 2:1–12. https://doi.org/10.3894/JAMES.2010.2.1
44. Lee CY, Camargo SJ, Sobel AH, Tippett MK (2020) Statistical-dynamical downscaling projections of tropical cyclone activity in a warming climate: two diverging genesis scenarios. J Clim 33:4815–4834. https://doi.org/10.1175/JCLI-D-19-0452.1
45. Tippett MK, Camargo SJ, Sobel A (2011) A poisson regression index for tropical cyclone genesis and the role of large-scale vorticity in genesis. J Clim 24:2335–2357. https://doi.org/10.1175/2010JCLI3811.1
46. Nolan DS, Rappin ED (2008) Increased sensitivity of tropical cyclogenesis to wind shear in higher SST environments. Geophys Res Lett 35:L14805. https://doi.org/10.1029/2008GL034147
47. Murakami H, Li T, Peng M (2013) Changes to environmental parameters that control tropical cyclone genesis under global warming. Geophys Res Lett 40(10):2265–2270. https://doi.org/10.1002/grl.50393
48. Vecchi GA et al (2019) Tropical cyclone sensitivities to CO_2 doubling: roles of atmospheric resolution, synoptic variability and background climate changes. Clim Dyn 53(9–10):5999–6033. https://doi.org/10.1007/s00382-019-04913-y
49. Tang B, Emanuel K (2012) A ventilation index for tropical cyclones. Bull Am Meteor Soc 93:1901–1912. https://doi.org/10.1175/BAMS-D-11-00165.1
50. Sugi M, Noda A, Sato N (2002) Influence of the global warming on tropical cyclone climatology. J Meteor Soc Jpn 80:249–272. https://doi.org/10.2151/jmsj.80.249
51. Tang B, Camargo SJ (2014) Environmental control of tropical cyclones in CMIP5: a ventilation perspective. J Adv Model Earth Syst 6:115–128. https://doi.org/10.1002/2013MS000294
52. Tam CY, Li T (2006) The origin and dispersion characteristics of the observed summertime synoptic-scale waves over the western Pacific. Mon Weather Rev 134:1630–1646. https://doi.org/10.1175/MWR3147.1
53. Li T, Kwon M, Zhao M, Kug JJ, Luo JJ, Yu W (2010) Global warming shifts Pacific tropical cyclone location. Geophys Res Lett 37:L21804. https://doi.org/10.1029/2010GL045124
54. Hsieh T-L, Vecchi GA, Yang W, Held IM, Garner ST (2020) Large-scale control on the frequency of tropical cyclones and seeds: a consistent relationship across a hierarchy of global atmospheric models. Clim Dyn 55:3177–3196. https://doi.org/10.1007/s00382-020-05446-5
55. Sugi M, Yamada Y, Yoshida K, Mizuta R, Nakano M, Kodama C, Satoh M (2020) Future changes in the global frequency of tropical cyclone seeds. Sci Online Lett Atmos 16:70–74. https://doi.org/10.2151/sola.2020-012